

Published in final edited form as:

Int J Biomed Nanosci Nanotechnol. 2013 ; 3(1-2): . doi:10.1504/IJBNN.2013.054508.

Protein expression profiles of intestinal epithelial co-cultures: effect of functionalised carbon nanotube exposure

Xianyin Lai,

Department of Cellular and Integrative Physiology, Indiana University School of Medicine, 1345 West 16th Street, Indianapolis IN 46202, USA, xlai@iupui.edu

Bonnie L. Blazer-Yost,

Department of Cellular and Integrative Physiology, Indiana University School of Medicine, 1345 West 16th Street, Indianapolis IN 46202, USA and Department of Biology, Indiana University-Purdue University Indianapolis, 723 West Michigan Street, Indianapolis IN 46202, USA, bblazer@iupui.edu

James W. Clack,

Department of Biology, Indiana University-Purdue University Columbus, 4601 Central Avenue, Columbus IN 47203, USA, jclack@iupui.edu

Sharry L. Fears,

Sensient Bio-Ingredients, 5600 West Raymond Street, Indianapolis IN 46241, USA, sharry.fears@sensient.com

Somenath Mitra,

Department of Chemistry and Environmental Science, New Jersey Institute of Technology, Newark NJ 07102, USA, somenath.mitra@njit.edu

Susana Addo Ntim,

Department of Chemistry and Environmental Science, New Jersey Institute of Technology, Newark NJ 07102, USA, sa57@njit.edu

Heather N. Ringham, and

Department of Cellular and Integrative Physiology, Indiana University School of Medicine, 1345 West 16th Street, Indianapolis IN 46202, USA, hringham@iupui.edu

Frank A. Witzmann

Department of Cellular and Integrative Physiology, Indiana University School of Medicine, 1345 West 16th Street, Indianapolis IN 46202, USA, fwitzman@iupui.edu

Abstract

To assess the biological effects of low level, water dispersible, functionalised carbon nanotube (f-CNT) exposure in an in vitro model simulating the digestive tract, cellular protein expression was quantified and compared using label-free quantitative mass spectrometry (LFQMS). Co-cultured cells were exposed to well-characterised SWCNT-COOH, MWCNT-COOH, and MWCNT-PVP. The relative expression of 2,282 unique proteins was compared across the dose groups. 428 proteins were found to be differentially expressed. At the high dose, the extent of differential protein expression was CNT-specific and directly related to CNT colloidal stability. Cells responded to low level MWCNT-PVP exposure with three-fold greater differential expression.

Correspondence to: Frank A. Witzmann.

Supplemental data

Supplemental Figure 1 and Tables 1 to 10 can be downloaded from: <http://www.proteomics.iupui.edu/publications.html> or from the author by e-mail request: fwitzman@iupui.edu.

Bioinformatic analysis indicated significant and f-CNT-specific effects on relevant molecular and cellular functions and canonical pathways, with little overlap across f-CNT type and in the absence of overt toxicity.

Keywords

carbon nanotube; CNT; colon; in vitro; intestinal cells; label-free quantitation; mass spectrometry; poly(4-vinylpyrrolidone); proteomics

1 Introduction

Comprehensive analysis of differential protein expression can be utilised to derive molecular profiles to explain the complex biological effects of disease and injury (Amacher, 2010; Kyu Kim et al., 2011; Veenstra, 2011). In this regard, proteomic efforts using label-free quantitative mass spectrometry (LFQMS) have emerged as capable and reliable approaches to gain relevant and meaningful information at the protein level (Helsens et al., 2011; Neilson et al., 2011). LFQMS has recently been applied to toxicological investigations (Chiu et al., 2010; Osman et al., 2010; Sari et al., 2010; Lai et al., 2011), including the assessment of nanoparticle effects (Blazer-Yost et al., 2005; Teeguarden et al., 2011). In our efforts to investigate the molecular basis for the biological effects of nanoparticle exposure, we have developed a protein expression database for an *in vitro* model of the intestinal epithelial barrier exposed to well-characterised, water dispersible functionalised carbon nanotubes (f-CNTs): carboxylated single-walled carbon nanotubes (*SWCNT-COOH*) and multi-walled carbon nanotubes (*MWCNT-COOH*) and poly(4-vinylpyrrolidone) (PVP) wrapped multi-walled (*MWCNT-PVP*).

Carbon nanotubes (CNTs) possess unique electrical, mechanical, and thermal properties with potential applications in the electronics, catalysts, polymer composites, aerospace, and other industries. CNTs also are being developed for a broad range of applications in biomedicine, such as targeted drug delivery (including oral) (Nahar et al., 2006; Ito et al., 2007; Kateb et al., 2007), tissue engineering (Veetil and Ye, 2009; Zhang et al., 2010b), and miniaturised biosensors (Veetil and Ye, 2007; Zhang et al., 2010a). An important consequence of anticipated mass production and widespread application of potentially hazardous CNTs is the increased likelihood of occupational, environmental, and clinical exposure (Maynard et al., 2004; Borm et al., 2006; Lam et al., 2006) and potential for exposure-related inflammation, human illness, and dysfunction. Due to their small size and unique physicochemical properties, CNTs may interfere with normal biological processes when exposed to human cells (Donaldson et al., 2006; Simeonova, 2009).

In general, functionalisation generates new classes of CNT-based materials with physical, chemical and biological properties different from their non-functionalised precursors. Functionalisation also alters their fate in the environment, as well as their potential toxicity. For example, while raw, unrefined, and hydrophobic CNTs tend to settle out of aqueous media/environs into the sediment (Kennedy et al., 2008), highly water dispersible f-CNTs can contaminate water resources. We expect that large quantities of these derivatised forms of f-CNTs will be manufactured as they find diverse applications ranging from polymer composites to food packaging to oral drug delivery. Additional f-CNTs liberated from discarded products will find their way from landfills or other environs into ground water.

Consequently, one of the major potential routes of human exposure is alimentary, occurring via consumption of water or through food chain dynamics from products from plants and animals that have taken up the f-CNTs. Furthermore, inhaled CNT cleared by the

mucociliary escalator can be swallowed and enter the gastrointestinal (GI) tract (Oberdorster et al., 2005; Borm et al., 2006; Nel et al., 2006). CNTs functionalised for oral drug delivery provide another, potentially significant avenue for GI exposure and untoward effects. Therefore, f-CNTs from several principle sources, ingested or inhaled, either inadvertently or intentionally (oral drug delivery), can be expected to enter the digestive tract and exert biological effects on its barrier epithelia.

Despite this potential for GI exposure, only a few previous studies have investigated the effect of CNTs on Caco-2 cell monolayers (Kulamarva et al., 2008; Jos et al., 2009; Piovesan et al., 2010; Ponti et al., 2010; Coyuco et al., 2011) and HT29 monolayers (Pelka et al., 2011), and only two *in vivo* studies examined the toxicity of SWCNT in the intestine after oral gavage (Folkmann et al., 2009; Kolosnjaj-Tabi et al., 2010). A recent review does not even address GI effects (Johnston et al., 2010), since little is known about the biological effects of CNTs or f-CNTs in that regard. What is known about them is often contradictory (Krug and Wick, 2011). For example, sodium cholate dispersed SWCNTs have recently been shown to elevate reactive oxygen species (ROS) in HT29 cells exposed to 100 ng/mL for 3 h, concomitant with mitochondrial injury observed at 24 h (Pelka et al., 2011). In that same study, DNA damage was observed in exposures as low as 50 pg/mL.

By contrast, when colony forming efficiency was used as a sensitive measure of cytotoxicity, Caco-2 cells exposed to unrefined MWCNT were relatively unaffected by exposures as high as 100 µg/mL (Ponti et al., 2010). Jos et al. (2009) reported cytotoxicity in Caco-2 monolayers exposed to SWCNT-COOH only at exposures > 100 µg/mL. Similarly, sodium chitosan decorated SWCNT exposure at levels up to 10 mg/mL had only minor effect on Caco-2 cell viability (Piovesan et al., 2010). *In vitro* barrier function in Caco-2 monolayers has been shown to be impaired by SWCNT-COOH exposure, as indicated by reduced transepithelial electrical resistance (TEER) and increased lucifer yellow paracellular flux (Coyuco et al., 2011), but only at very high exposures (> 500 µg/mL). One might question whether the high concentrations used in these latter studies adequately simulate realistic levels of accidental oral exposure to f-CNTs.

When proteomic analyses of *in vitro* intestinal models have been applied, they have been limited to single cell-type monolayers and electrophoretic analytical platforms, with few exceptions. To provide a more relevant culture system and a more comprehensive proteomic platform, the present study used a well-characterised *in vitro* Caco-2/HT29-MTX co-culture model simulating the large intestine. Caco-2 and HT29-MTX adenocarcinoma cell lines are derived from intestinal absorptive and mucus-secreting goblet cell (Lesuffleur et al., 1991) types, respectively. Their combination provides a physiologically relevant co-culture system characterised by tight junctions and considerable mucus secretion (Walter et al., 1996; Hilgendorf et al., 2000; Mahler et al., 2009a, 2009b) that covers the entire monolayer.

Using this co-culture model and an innovative, label-free quantitative mass spectrometric (LFQMS) platform recently developed in our laboratory (Lai et al., 2011), we present significant effects of exposure to very low concentrations of f-CNT (500 pg/mL) on cellular protein expression, in the absence of overt toxicity, and link these changes to specific pathways and molecular functions that have physiological relevance.

2 Material and methods

2.1 Chemicals

DL-Dithiothreitol (DTT), urea, triethylphosphine, iodoethanol, and ammonium bicarbonate were purchased from Sigma-Aldrich (St. Louis, MO, USA). LC-MS grade 0.1% formic acid in acetonitrile and 0.1% formic acid in water were purchased from Burdick & Jackson

(Muskegon, MI, USA). Modified sequencing grade porcine trypsin was obtained from Princeton Separations (Freehold, NJ, USA).

2.2 CNTs and functionalisation

SWCNT were purchased from Unidym (Sunnyvale, CA) and MWCNT were purchased from Cheap Tubes Inc. (Brattleboro, VT). SWCNT-COOH and MWCNT-COOH were generated in a Microwave Accelerated Reaction System (Mode: CEM Mars) fitted with internal temperature and pressure controls as previously described (Chen et al., 2007; Chen and Mitra, 2008). Pre-weighed amounts of purified MWCNT were treated with a mixture of concentrated H_2SO_4 and HNO_3 solution by subjecting them to microwave radiation at 140°C for 20 min. The product was filtered through a $10\ \mu\text{m}$ membrane filter, washed with water to a neutral pH, and dried under vacuum at 80°C to a constant weight. SWCNT-COOH was also functionalised in the Microwave Accelerated Reaction System according to a procedure developed by our team (Wang et al., 2005). Pre-weighed amounts of purified SWCNT were treated with a 1:1 mixture of concentrated H_2SO_4 and HNO_3 solution by subjecting them to microwave radiation at 120°C for 3 min. The mixture was then diluted with distilled water and filtered through $10\ \mu\text{m}$ membrane filter paper. The filtrate was transferred to a dialysis bag and placed in a container filled with DI water, which was continually replaced until it achieved neutral pH. The filtrate was then dried overnight at 50°C under vacuum. This led to the formation of carboxylic acid groups on the surface of the CNTs resulting in high aqueous dispersibility. MWCNT-PVPs were prepared according to a procedure previously reported by Ntim et al. (2011). Purified MWCNTs were dispersed in deionised water at a concentration of $50\ \text{mg/L}$ with the aid of 1% sodium dodecyl sulphate (SDS). 1% by weight of PVP was added to the mixture, which was then incubated at 50°C for 12 hours. The CNTs were then filtered through a $10\ \mu\text{m}$ membrane filter, washed with deionised water followed by three cycles of ultrasonic redispersion in deionised water to remove any residual SDS. The sample was filtered and dried under vacuum at room temperature to a constant weight.

2.3 Characterisation of the f-CNTs

The materials were characterised by scanning electron microscope (SEM) and Fourier transform infrared spectroscopy (FTIR). SEM data was collected on a LEO 1530 VP SEM equipped with an energy-dispersive X-ray analyser. FTIR measurements were carried out in purified KBr pellets using a Spectrum One FT-IR Spectrometer (Perkin-Elmer). Zeta-potential measurements of the f-CNT suspensions were performed using a ZetaSizer Nano-ZS Instrument (Malvern Instruments, Worcestershire WR, UK). The relative hydrodynamic size of the f-CNTs suspended in deionised water was measured using dynamic light scattering at 90° . A kinetic analysis of f-CNT suspension stability and sedimentation was performed by monitoring the absorbance of phenol-red free culture media at $550\ \text{nm}$ using UV-vis spectrophotometry (Cary 300 UV-visible spectrophotometer, Varian, Palo Alto CA) (Wang et al., 2010). $1\ \text{mL}$ of each f-CNT suspension at $10\ \mu\text{g/mL}$ was prepared and OD measurements taken at 0, 3, 24, and 48 h. The $500\ \text{pg/mL}$ was too dilute; therefore, the stability of that suspension could not be assessed. To examine aggregate formation via agglomeration, bundling, and entanglement of f-CNTs at the cell monolayer surface ($10\ \mu\text{g/mL}$ exposures), bright field images were acquired using an IX71 microscope (Olympus, Center Valley PA) equipped with a $10\times/0.4$ objective lens. The microscope was coupled to an Orca R2 Deep cooled CCD camera (Hamamatsu, Bridgewater NJ). The $1,344$ by $1,024$ pixel images were processed using ImageJ software (NIH).

2.4 Cells, co-culture, and exposures

Caco-2, human colorectal adenocarcinoma cells (ATCC HTB-37, Lot 57863838) were maintained in Eagle's minimal essential medium (EMEM) supplemented with 10% FBS

(ATCC catalogue #s 30-2003 and 30-2020) and incubated at 37°C – 5% CO₂. HT29-MTX, human colon adenocarcinoma cells treated with methotrexate (Lesuffleur et al., 1993), were obtained from Dr. Thécia Lesuffleur (INSERM, Paris, France) and were maintained in Dulbecco's Modified Eagle's Medium (DMEM) with glutamax and 10% heat inactivated fetal bovine serum (Invitrogen, Carlsbad CA) at 37°C – 5% CO₂. Both cell lines were sub-cultured at 80% to 90% confluence. Caco-2 (passages 49 and 63) and HT29-MTX cells (passages 29 and 33) were cultured to obtain several Corning T75 flasks. At 80% to 90% confluence, the cells were trypsinised and flasks were pooled. Cells were counted using a hemocytometer and then mixed together at a 75:25 Caco-2 to HT29-MTX ratio and placed in the HT29-MTX medium with 1% penicillin-streptomycin. Combined cells were mechanically mixed and 1 mL was added to six-well Transwell™ inserts to obtain 0.4×10^6 cells per well (8.9×10^4 cells/cm²) (Hilgendorf et al., 2000).

Cells were incubated at 37°C – 5% CO₂ for 14 days prior to exposure, replacing the medium every other day, to achieve full, post-confluent differentiation, polarisation, and tight-junction formation. SWCNT-COOH, MWCNT-COOH, and MWCNT-PVP were weighed and added to autoclavable glass tubes with screw caps; water was added to make a 6 mg/mL suspension. The f-CNTs were gently sonicated using a Branson Sonifer S-250A (Danbury CT) with a microtip. The sonication settings were output control 3, duty cycle 30% for 20 pulses per sample. Immediately after sonication, an aliquot was removed for serial dilution in water to prepare the following stock solutions: 3,000 µg/mL, 300 µg/mL, 15 µg/mL, 1.5 µg/mL, 0.15 µg/mL, and 0.015 µg/mL. Each sample was then sonicated before dilution to the next concentration. Prior to cell exposure the f-CNT samples were autoclaved, sonicated in a water bath sonicator for 5 minutes, and vortexed for 20 to 30 seconds. Immediately, a 1.2 mL aliquot of the NP stocks (0.015, 0.15, 300, 3,000 µg/mL) was diluted in 34.8 mL of HT29-MTX medium (DMEM) to a final concentration of 500 µg/mL, 5 ng/mL, 500 ng/mL and 10 µg/mL. Cadmium oxide was used as a positive control⁴⁹ at a final 20 µg/mL concentration. The f-CNT doses were chosen to correspond to typical *in vitro* exposures appearing the literature (Zhang et al., 2008; Jos et al., 2009; Ponti et al., 2010; Pelka et al., 2011). The minimal dose range was chosen to simulate potential dilution effects of environmental contamination and in view of our previous observations of low-dose effects in kidney and airway epithelial cells (Blazer-Yost et al., 2011; Banga et al., 2012).

The final f-CNT mixtures were gently sonicated, vortexed quickly, and 1.5 mL placed in the top (apical) compartment of the 6 Transwell™ plate containing the co-cultured cells. The bottom (basolateral) compartment contained 2.5 mL of fresh medium. Control groups received only fresh medium in both compartments. The treated cells were incubated for 48 hours at 37°C – 5% CO₂. This time point was chosen to simulate potential long-term bioavailability related to the copious mucus layer in which f-CNTs may be trapped. To assess cell number at exposure, co-cultured cells were trypsinised and counted using a hemocytometer (n = 4) after 16 days. Cell counts indicated a total of ~750,000 cells per Transwell™ insert.

2.5 Transepithelial electrical resistance

As mentioned earlier, cell co-cultures were grown for 14 days on Transwell™ inserts to achieve full, post-confluent differentiation, polarisation, and tight-junction formation. To assess the latter, the filters were excised, mounted in an Ussing chamber, and connected to a DVC-1,000 voltage/current clamp (World Precision Instruments, Sarasota FL) with voltage and current electrodes on either side of the membrane as described in detail previously (Shane et al., 2006). The spontaneous transepithelial potential difference was clamped to zero, and the resultant short-circuit current (SCC) was monitored continuously. The cells were bathed in serum-free medium maintained at 37°C via water-jacketed buffer chambers on either side of the filter. Medium was circulated and kept at constant pH using a 5%

CO₂/95% O₂ gas lift. TEER was recorded every 200 seconds throughout each experiment by applying a 2 mV pulse and the resulting deflection in the SCC was measured and used to calculate the TEER by Ohm's law.

2.6 Cytokine analysis

To determine the level of irritation or inflammation associated with CNT exposure after 8 h, cell culture medium was collected from apical and basolateral compartments of the Transwell™ plates and evaluated for IL-1, IL-6, IL-8, IL-10, and TNF- α by ELISA using cytokine Colorimetric kits (R&D Systems, Inc., Minneapolis MN) following the manufacturer's instructions. These cytokines are known to be expressed constitutively by both Caco-2 and HT29 cells according to the gene expression omnibus (GEO) database (Edgar et al., 2002), which stores individual gene expression profiles from curated data sets in its repository.

2.7 Cell viability, membrane integrity, oxidative stress, and permeability assays

In assays that produce insoluble formazan dyes (such as the MTT assay), CNTs attach to the insoluble MTT formazan product disrupting the distinguishing, colorimetric reaction (Worle-Knirsch et al., 2006). Therefore, assays that produce soluble dyes such as XTT are preferred. Accordingly, cell viability was determined using the cell proliferation kit (Roche, Indianapolis IN) according to manufacturer instructions.

- *LDH assay.* Membrane leakage of LDH from potentially damaged or dead cells was assessed using the CytoTox 96 Non-Radioactive Cytotoxicity Assay (Promega, Fitchburg WI) according to the manufacturer's instructions.
- *Oxidative stress assay.* Generation of ROS by exposed cells was measured using the OxiSelect ROS assay (Cell Biolabs, San Diego CA) according to the manufacturer's instructions. This assay uses the plasma membrane-permeable fluorogenic probe, 2',7'-dichlorodihydrofluorescein diacetate (DCFH-DA), whereby the observed fluorescence intensity of 2',7'-dichlorofluorescein (DCF) is proportional to the ROS levels within the cells.
- *Cell permeability assay.* Epithelial barrier function was assessed by measuring unidirectional paracellular flux of lucifer yellow from the apical to basolateral compartments. This assay was conducted via the Lucifer Yellow Permeability Assay (BD Biosciences, Franklin Lakes NJ) according to the manufacturer's instructions, using Transwell™ cultures as described above.

2.8 Proteomics work flow

Due to the complexity of the label-free quantitative mass spectrometric proteomic analysis and the data volume produced, protein expression profiling was limited to only the low and high f-CNT exposures, and thus a complete dose-response analysis was not attempted at this time. After incubation of the exposed cells, the media from both compartments were individually removed, placed into separate labelled microfuge tubes, snap frozen in liquid nitrogen, and placed on dry ice until transfer to a -80°C freezer for cytokine analysis. The Transwell™ membranes containing adherent cells were quickly rinsed three times in ice-cold 250 mM sucrose, snap frozen in liquid nitrogen, placed on dry ice, and then stored at -80°C. For Caco-2/HT29-MTX lysate preparation, 500 μ L of lysis buffer (8 M urea, 10 mM DTT freshly prepared) was added to each sample. All cells were incubated at 35°C for 1 hour with agitation, transferred to an ultracentrifuge tube, and briefly vortexed. Cell lysates were centrifuged at 100,000 \times g for 20 min at 4°C to remove the mucus gel and insoluble materials and then transferred to an Ultrafree-MC Centrifugal Filter Unit (Millipore, Billerica, MA) and centrifuged at 3,500 \times g for 8 min at room temperature for final cleanup.

Fully solubilised cell protein samples were then stored at -80°C until analysis. Protein concentration was determined by the Bradford Protein Assay using Bio-Rad (Hercules CA) protein assay dye reagent concentrate. A 100 μg aliquot of each sample was adjusted to 200 μL with 4 M urea and then reduced and alkylated by triethylphosphine and iodoethanol as described previously (Lai et al., 2008). A 150 μL aliquot of a 20 $\mu\text{g}/\text{mL}$ trypsin solution was added to the sample and incubated at 35°C for 3 h, after which another 150 μL of trypsin was added, and the solution incubated at 35°C for 3 h ($n = 5$ per observation). Exactly 20 μg of each tryptic digest sample ($n = 5$) were injected randomly as two technical replicates onto a C18 reversed phase column (TSK gel ODS-100V, 3 μm , 1.0 mm \times 150 mm) at a flow rate of 50 $\mu\text{L}/\text{min}$ as part of the Surveyor autosampler and MS HPLC system (Thermo-Electron, Waltham MA) coupled to a Thermo-Finnigan linear ion-trap (LTQ) mass spectrometer. The mobile phases A and B were 0.1% formic acid in water and 50% ACN with 0.1% formic acid in water, respectively. The gradient elution profile was as follows: 10% B (90% A) for 10 min and 10% to 100% B (90.0% A) for 170 min. The spectral data were collected in the 'data dependent MS/MS' mode with the ESI interface using a normalized collision energy of 35%. Dynamic exclusion settings were repeat count 1, repeat duration 30 s, exclusion duration 120 s, and exclusion mass width 0.6 m/z (low) and 1.6 m/z (high). A blank was injected between each sample to clean and balance the column and to eliminate carryover. The acquired data were searched against the International Protein Index (IPI) database (ipi.HUMAN.v3.76) using SEQUEST (v. 28 rev. 12) algorithms in Bioworks (v. 3.3). General parameters were set to: peptide tolerance 2.0 amu, fragment ion tolerance 1.0 amu, enzyme limits set as 'fully enzymatic – cleaves at both ends', and missed cleavage sites set at 2. Peptide and protein identifications were validated by PeptideProphet (Keller et al., 2002) and ProteinProphet (Nesvizhskii et al., 2003) in the trans-proteomic pipeline (TPP, v. 3.3.0) (<http://tools.proteomecenter.org/software.php>). Only proteins and peptides with:

- a. protein probability 0.9000
- b. peptide probability 0.8000
- c. peptide weight 0.5000 were used in the quantitation algorithm.

Protein abundance was determined using IdentiQuantXL™ (Lai et al., 2011). Briefly, after chromatogram alignment and peptide retention time determination, a weighted mean m/z of each peptide was calculated and a tab delimited file was created to extract peptide intensity using MASIC (Monroe et al., 2008). Peptides were then filtered according to intensity CV across all samples and intensity correlation, for those identifying a particular protein. Protein abundance was then calculated from all qualified corresponding peptides matched to that protein.

2.9 Statistical analysis and bioinformatics

Comparison of the abundance of individual protein dose-group means generated by LFQMS was performed within the IdentiQuantXL™ platform using one-way ANOVA and pairwise multiple comparisons (Holm-Sidak method). Critical F-ratio significance for ANOVA was set at $p < 0.01$ and pairwise comparison at $p < 0.05$. False discovery rate (FDR) (Storey, 2002) was estimated using Q-value software. Statistical comparisons of toxic endpoint data were accomplished via ANOVA and *post hoc* pairwise multiple comparisons (Holm-Sidak method) (SigmaPlot, Systat Software, Inc., Chicago IL). To interpret the biological relevance of the differential protein expression data and to compare biological effects across different f-CNTs and exposure levels, protein lists and their corresponding expression values (fold change) were uploaded onto the Ingenuity Pathway Analysis (IPA) software server (<http://www.ingenuity.com>) and analysed using the core analysis module to rank the proteins into top molecular and cellular functions and canonical pathways. The IPA functional analysis identified the biological functions that were most significantly related to

the protein dataset. Differentially expressed proteins from the dataset that were associated with biological functions in ingenuity's knowledge base were considered for the analysis. Right-tailed Fisher's exact test was used to calculate a p-value determining the probability that each biological function assigned to that dataset is due to chance alone. The canonical pathways analysis identified the pathways from IPA's library of canonical pathways that were most significantly related to the dataset. As above, differentially expressed proteins from the dataset that were associated with a canonical pathway in ingenuity's knowledge base were considered for the analysis. The significance of the association between the protein dataset and the canonical pathway was measured in two ways:

1. A ratio of the number of molecules from the dataset that map to the pathway divided by the total number of molecules that map to the canonical pathway is displayed.
2. Fisher's exact test was used to calculate a p-value determining the probability that the association between the genes in the dataset and the canonical pathway is explained by chance alone.

3 Results

3.1 Co-culture

The co-culture system is illustrated in the electron micrographs shown in Figure 1. Fully differentiated Caco-2 (brush border) and HT29-MTX (mucus secreting) cells are clearly visible. Tight junctions characteristic of a fully functional barrier epithelium monolayers are also apparent. The electrophysiological consequence of tight-junction formation, a moderately high resistance monolayer, is illustrated in this figure by TEER measurements that are consistent with previous observations using this culture system (Chen et al., 2010).

3.2 CNT characterisation

Physicochemical characteristics of the f-CNTs are listed in Table 1. Their structure was analysed by SEM and FTIR spectroscopy and these results are presented in Figure 2. The SEM images show that the tubes remained intact after acid treatment with minimal visible tube damage [Figure 2(a)]. It is apparent from the SEM images of MWCNT-PVP that the PVP was uniformly distributed on the nanotubes and the latter retained its morphology. The FTIR spectrum shown in Figure 2(b), confirmed the presence of functional groups in the f-CNTs. The carboxylic stretching frequency in the carboxylated CNTs occurred at 1,715 cm^{-1} and 1,724 cm^{-1} for MWCNT-COOH and SWCNT-COOH respectively, with the stretching (O-H) vibration occurring around 3,440 cm^{-1} . The C-O stretching frequency occurred at 1,225 and 1,230 cm^{-1} for MWCNT-COOH and SWCNT-COOH, respectively. The carbonyl stretching frequency from the amide group in PVP occurred at 1,645 cm^{-1} . In the MWCNT-COOH and MWCNT-PVP spectra, the peak around 1,576 cm^{-1} was assigned to the C=C stretching of the carbon skeleton, this occurred at 1,620 cm^{-1} for SWCNT-COOH. Table 1 lists the zeta potential as well as particle size in aqueous suspension. Despite functionalisation and enhanced dispersibility, at 10 $\mu\text{g/mL}$ all CNTs exhibited agglomeration [Figure 3(a)]. From the cell surface photomicrographs, agglomerant size measurements ranged from 3 μm spherical to 10 $\mu\text{m} \times 50 \mu\text{m}$ oblong, with nothing larger detected. At the 500 pg/mL exposure (not shown), agglomerants were completely absent and images resembled the control shown in Figure 3(a). Colloidal stability in the culture medium, when plotted against the overall effect of the f-CNT (10 $\mu\text{g/mL}$) on protein expression [Figure 3(b)], suggests that the least stable MWCNT-COOH (which displayed the most extensive agglomeration) had the greatest effect, while the most stable SWCNT-COOH (which displayed the least agglomeration) has the least affect at this exposure. The

comparative behaviour of MWCNT-COOH and MWCNT-PVP confirms our previous observations concerning their stability in aqueous dispersions (Ntim et al., 2011).

3.3 Cytokine analysis, cell viability, membrane integrity, permeability assay, and oxidative stress

Apical and basolateral culture media levels of IL-1, IL-6, IL-8, IL-10, and TNF- were unaffected by f-CNT exposure, with one exception. MWCNT-COOH exposure at 500 pg/mL caused a 2.5-fold elevation in apical IL-8 (Figure 4). Comparatively, the CdO positive control exposure resulted in an 18-fold increase in this cytokine. Cell viability measured by the XTT assay [Figure 5(a)], was unaffected by f-CNT exposure, as was cell membrane integrity, as measured by LDH release [Figure 5(b)]. By contrast, exposure to 20 µg/mL of CdO resulted in a 40% to 60% loss in viability. Exposure to f-CNT had no significant effect on epithelial barrier integrity, as shown in Figure 5(c) where lucifer yellow paracellular flux remained essentially unaltered. Only in the CdO positive control was the barrier compromised. Consistent with all the observations above, no significant ROS generation was observed in any f-CNT exposures (Figure 6).

3.4 Differential protein expression

To define and compare the Caco-2/HT29-MTX proteome in various f-CNT exposure groups, a LFQMS-based approach was used to identify and quantify proteins expressed by the co-cultured cells. A total of 8,081 unique peptides were identified across all co-culture protein samples, leading to the identification and quantification of 4,743 proteins, representing 2,282 unique cellular proteins, splice variants, or isoforms. This database, including MS supporting information, is presented in Supplemental Table 1 (see Supplemental data). It represents the most comprehensive intestinal epithelial cell protein expression profile of its kind to date (Hardwidge et al., 2004; Nanni et al., 2009).

Whereas gene expression analysis via microarray and proteomic analysis using stable isotope-tagged or coded peptides enables expression comparisons by comparative ratios and fold differences, the platform used here enables relative protein quantitation based on peptide ion intensity. Consequently, highly abundant proteins have elevated ion intensities, enabling one to compare expression statistically and determine which proteins are in relatively high or low abundance. Accordingly, the top 50 proteins, in terms of relative abundance, in the database are presented in Supplemental Table 2 (see Supplemental data).

Differential protein expression (ANOVA $p < 0.01$) and *post hoc* multiple comparisons (by Holm-Sidak $p < 0.05$) of group-wise means for all 2,282 proteins were made between exposure and control groups. In this regard, the abundance of 428 unique proteins (17.5%) significantly differed across the various f-CNT treatments. The exposure-related effects are summarised in Figure 7 and specific lists of the differentially expressed proteins associated with each exposure are provided in Supplemental Table 3 to Supplemental Table 8 (see Supplemental data). At the high-dose exposure (10 µg/mL) MWCNT-COOH treatment affected the greatest number of proteins, 118, followed by MWCNT-PVP (83) and SWCNT-COOH (33). This relationship is consistent with and significantly correlated to the stability of the f-CNTs in the culture media (Figure 3). As mentioned earlier, micron-size f-CNT agglomerant formation and settling at 10 µg/mL was greatest in MWCNT-COOH and least in SWCNT-COOH. At this dose, protein alterations may be a consequence of these size-related phenomena. At the 500 pg/mL MWCNT-PVP dose, where nanotubes appear to be relatively free and non-agglomerated, 'nano-effects' may account for the observed alterations, similar to quantum dot effects in Caco-2 cells observed previously (Koeneman et al., 2009), where aggregates had less biological effect than free particles. The overall pattern of change in protein expression change at this dose was consistent among the functionalised

MWCNT, 80% and 78% of the altered proteins were down-regulated in MWCNT-COOH and MWCNT-PVP, respectively. By contrast, 64% of the proteins altered by SWCNT-COOH exposure at 10 $\mu\text{g}/\text{mL}$ were up-regulated.

At the very low level exposure (500 pg/mL) MWCNT-PVP treatment affected the expression the greatest number of proteins, 256, followed by MWCNT-COOH (109) and SWCNT-COOH (13). All of the proteins altered by SWCNT-COOH were down-regulated while MWCNT-COOH exposure down-regulated 87% of the altered proteins. In striking contrast, 97% of the proteins altered by 500 pg/mL MWCNT-PVP exposure were up-regulated. More remarkable is the observation that the 500 pg/mL exposure had an effect on protein expression more than three-fold greater than the 10 $\mu\text{g}/\text{mL}$ exposure, a 20,000-fold higher dose.

Among the diverse protein alterations, the expression of 14 unique proteins was consistently altered by all f-CNTs (Table 2). The heterogeneity of f-CNT and exposure effects on the Caco-2/HT29-MTX proteome is illustrated in the Venn diagrams shown in Figure 8.

3.5 Exposure effects on molecular and cellular functions and canonical pathways

To interpret the biological relevance of the differential protein expression data and to compare biological effects across different f-CNTs and exposure levels, protein alterations were studied by IPA. Molecular and cellular functions and canonical pathways statistically matched to groups of differentially expressed proteins are listed in Supplemental Tables 9 and 10 (see Supplemental data). Interrelationships between these effects and f-CNT exposures are illustrated in Figures 9 and 10.

4 Discussion

In view of the potential for human GI tract exposure to functionalised, water dispersible CNTs through intentional, accidental or even inhalatory means, the present study simulated the effect of oral exposure to f-CNTs and investigated their effect on the intestinal barrier using a novel co-culture system composed of brush border and goblet cell components, not previously used in nanotoxicology studies, combined with an improved LFQMS platform for global protein analysis. The exposure levels were selected to be physiologically and environmentally relevant, approximate those used previously in published studies, and to simulate the extensive dilution one might expect from groundwater or food chain contamination. Based on several measures of cytotoxicity, irritation, and injury to the barrier cells, exposure to 500 pg/mL or 10 $\mu\text{g}/\text{mL}$ for 48 h had no apparent adverse effects. Absence of generalised cytokine release may be related to the duration of exposure. Early cellular irritation and inflammatory responses may ameliorate after this length of time and thus be undetectable. Alternatively, cytokine production may be limited to specific effectors that were not measured in our standardised inflammatory cytokine panel. Similarly, absence of ROS at 48 h does not preclude their elevation at earlier time points, as previously observed (Pelka et al., 2011). Nevertheless, the overall lack of toxicity is consistent with previous observations where low dose CNT exposures to either Caco-2 or HT29 epithelia failed to elicit overt toxicity, compared to excessively high doses, which did (Jos et al., 2009; Piovesan et al., 2010; Ponti et al., 2010; Coyuco et al., 2011). A possible explanation for these observations is that the static mucus layer, that is characteristic of the co-culture system used in this study, offers a certain degree of protection to the epithelial layer (Mrsny, 2009). In this model system, the mucus layer may thus protect against the cytotoxic effects of CNT exposure at low doses observed by Pelka et al. (2011) but over the 48 h incubation and exposure, it may be insufficient to avoid cellular effects appearing as changes in the proteome. Despite the lack of overt toxicity observed, global protein expression analysis

revealed significant effects of exposure and unique protein expression profiles for each f-CNT, with little overlap and few dose-response relationships.

4.1 The 50 most abundant proteins in the database

Not surprisingly, one of the most abundant proteins detected was mucin (MUC5AC). Mucin and strongly bound Fc-gamma binding protein (FcGBP) (Johansson et al., 2009) are known to be two major components of the colonic mucus barrier. Both were significantly decreased (~20% and ~15%, respectively) by exposure to all three f-CNTs at 10 µg/mL (but not 500 pg/mL), suggesting a CNT-associated down-regulation in the HT29-MTX (goblet cell) component of the co-culture (see Figure 1). Anterior gradient protein 2 homolog (AGR2), a protein disulfide isomerase required for mucin post-transcriptional synthesis and secretion (Park et al., 2009), myristoylated alanine-rich C-kinase substrate (MARCKS) a component of the secretory complex required for mucin granule exocytosis in airway goblets cells (Li et al., 2001), and MUC5B were all decreased by CNT exposure, though not significantly. Another mucin-associated protein, the 25th most abundant protein detected, endogenous galactoside-binding protein galectin-3 (LGALS3), which is expressed at higher levels in colon cancers than normal colon (Byrd and Bresalier, 2004), remained unaffected by f-CNT exposure.

From 20 different cytokeratins identified and quantified, KRT8, KRT19, KRT18, and KRT20 ranked 1st, 7th, 13th, and 32nd, respectively. KRT20 is highly expressed in colorectal carcinomas (Chu et al., 2000) while the others are characteristic of colonic epithelia *in vivo*, with KRT18 and 19 confined to the region of the crypts, KRT8 along the entire crypt-villus axis, and KRT20 in differentiated villus cells (Calnek and Quaroni, 1993) that correspond to the co-culture system used in this study. Of the above, only KRT18 was significantly affected by f-CNT exposure, where it was down-regulated by MWCNT-COOH at 10 µg/mL and up-regulated by MWCNT-PVP at 500 pg/mL. Additional highly expressed structure-related proteins include alpha actin, alpha-actinin 4, alpha and beta spectrin (four isoforms), alpha and beta tubulin, calcyclin, cofilin-1, myosin-9, neuroblast differentiation-associated protein AHNAK, prelamin A, profilin-1, and villin-1. Of these cytoskeletal proteins, the expression of only three was altered by f-CNT exposure. Alpha-actinin and cofilin 1 were up-regulated by MWCNT-PVP at 500 pg/mL while several isoforms of beta tubulin were both up- and down-regulated by both MWCNT-PVP exposures. Cofilin 1 was down-regulated by both MWCNT-COOH exposures.

Other prominently expressed proteins include those involved in energy metabolism: alcohol dehydrogenase, alpha enolase, creatine kinase, isocitrate dehydrogenase, glyceraldehyde-3-phosphate dehydrogenase, glycogen phosphorylase, phosphoglycerate kinase 1, pyruvate kinase M2, and triosephosphate isomerase. Of these metabolic proteins, enolase, the second most abundant protein detected was down-regulated only by the low-dose MWCNT-COOH exposure as were phosphoglycerate kinase I (and II) and triosephosphate isomerase. The latter protein was also down-regulated by MWCNT-PVP exposure at 10 µg/mL. Conversely, creatine kinase B and isocitrate dehydrogenase were up-regulated by low-dose MWCNT-PVP exposure.

4.2 Common protein expression effects exerted by all f-CNT exposures (except low dose SWCNT-COOH)

As mentioned earlier, emblematic of the heterogeneity of f-CNT effects, the expression of only 14 unique proteins was consistently altered by all f-CNTs (Table 2), with the exception of low-dose SWCNT-COOH. Despite a general absence of an f-CNT effect on inflammatory cytokine (interleukins and TNF-) release by the co-cultured cells, one protein that was up-regulated was macrophage migration inhibitory factor (MIF) (increased up to three-fold).

MIF is a ubiquitous protein that is found in virtually all cells and acts as an integral part of the host response to tissue invasion (Grieb et al., 2010). In the intestine, MIF acts as a pro-inflammatory cytokine specifically involved in the innate immune response to bacterial pathogens, has been shown to be constitutively expressed (Man et al., 2008) in Caco-2 and HT29 cells, is released predominantly from the apical side after Salmonella infection (Maaser et al., 2002), and its expression is correlated with susceptibility of the colon cells to apoptosis (Yao et al., 2005). MIF plays a role in M cell-mediated transport (and perhaps conversion of Caco-2 to M cells) and cross-talk between bacteria, gut epithelium, and immune system. MIF's up-regulation by f-CNT exposure, even at 500 pg/mL, indicates a proinflammatory effect at extraordinarily low doses and demonstrates a significant biological response common to all three f-CNTs. Expression of MIF has been shown to be increased in BEAS-2B cells by 20 µg/mL exposure to TiO₂ particles, carbon black, and diesel exhaust particles (Cha et al., 2007), a result replicated *in vivo*. MIF's consistent up-regulation observed here suggests cellular perturbation by all three f-CNTs in the absence of more conventional cytokine release.

Glucosamine-fructose-6-phosphate aminotransferase 2 (GFPT2) catalyses the formation of glucosamine-6-phosphate from fructose-6-phosphate and is the first rate-limiting enzyme of the hexosamine biosynthetic pathway. It controls the flux of glucose into the hexosamine pathway, thereby regulating the availability of precursors for N- and O-linked glycosylation of proteins. GFPT2's up-regulation may have implications regarding the observed down-regulation of both mucin (MUC5AC) and its associated FcGBP by all 10 µg/mL f-CNT exposures. It may be a compensatory response to the presence of f-CNT to increase the secretion of GI mucus, or immunoglobulin, or the secretory component of IgA, all of which contain large amounts of N-acetylglucosamine generated from UDP-N-acetylglucosamine. Nevertheless, increased expression of GFPT2 with 500 pg/mL f-MWCNT is difficult to interpret in terms of a mucus response because mucin expression was unaffected at those exposures. Though other members of the glucosamine metabolism family were detected and quantified, GFPT1 isoform (predominantly expressed in skeletal muscle), glucosamine-6-phosphate isomerase 1 (GNPDA1), N-acetylglucosamine-6-sulfatase (GNS), and UDP-N-acetylglucosamine transferase (ALG13), only GFPT2 expression was significantly altered.

Another cellular protein component, adaptor-related protein complex 1, gamma 2 subunit (AP1G2) was significantly increased by all exposures. AP1G2 is an important component of clathrin-coated vesicles that transport ligand-receptor complexes from the plasma membrane or from the trans-Golgi network to lysosomes and its actions in the endosomal pathway are ubiquitin-dependent (Rost et al., 2008). Though we have no evidence of f-CNTs at or in the plasma membrane (TEM analyses were unable to reveal the appearance of f-CNT at the plasma membrane or anywhere inside the cells), one might speculate that up-regulation of this adaptin component responds to the appearance of potential cargo (e.g., f-CNT) at the cell surface. The AP-1 adaptor protein (AP) complex is also a component of clathrin-coated vesicles associated with the trans-Golgi network. AP-1 is a heterotetramer composed of several adaptins, two large subunits (α and β), a medium-sized or μ subunit, and a small or γ subunit (Robinson and Bonifacino, 2001). An additional 19 functionally related proteins were identified, including the δ subunit of AP-1, which was also up-regulated significantly by PVP-MWCNT at 500 pg/mL. Others undergoing similar, though insignificant increases included phosphatidylinositol-binding clathrin assembly protein, vacuolar protein sorting-associated protein 26A, sortilin-related receptor, vesicle amine transport protein 1, and RAB11A. A number of clathrin heavy and light chains, vacuolar protein sorting-associated proteins, vesicle docking proteins, lectin mannose-binding 2, and charged multivesicular body protein were down-regulated, though not statistically significant. Changes in the endosomal pathway also may be part of a paracrine response to f-CNT-initiated MIF release (Arneson and Miller, 2007).

Carboxyl ester lipase (bile salt-stimulated lipase) (CEL) was consistently down-regulated by f-CNT exposure. This pancreatic digestive enzyme hydrolyses a wide variety of lipid substrates. According to the NCBI UniGene EST Profile database (<http://www.ncbi.nlm.nih.gov>), CEL is constitutively expressed in the intestine at low levels, and at much higher levels in colorectal tumours. In the intestine, it promotes large chylomicron production, catalyses fat and vitamin absorption, and acts in concert with pancreatic lipase and colipase for the complete digestion of dietary triglycerides. The impact of f-CNT-related down-regulation can only be speculated and may simply involve a reduced functional capacity of the colonic cells in response to the presence of unusual extracellular components such as nanotubes.

Succinate-CoA ligase (GDP-forming) beta subunit (SUCLG2) is a mitochondrial matrix enzyme that catalyses the reversible conversion of succinyl-CoA and ADP or GDP to succinate and ATP or GTP. Like CEL above, SUCL2 is constitutively expressed in the intestine, and at higher levels in colorectal tumours. The functioning ligase is composed of an α subunit, encoded by SUCLG1 (not detected in this study), and a β subunit, encoded by either SUCLA2 or SUCLG2. Both subunits are widely expressed in human tissues, with SUCLG2 predominantly expressed in anabolic tissues where it is critical for mtDNA maintenance (Miller et al., 2011). Though its consistent and uniform down-regulation by f-CNT is difficult to explain, SUCLG2's decreased expression may have important implications in mitochondrial function, particularly energy generation.

The expression of six histone isoforms was increased by all exposures except low-dose SWCNT-COOH, including six additional isoforms that were variably up-regulated by the 10 $\mu\text{g/mL}$ exposure [see Supplemental Figure 1 (Supplemental data)]. Histones are basic nuclear proteins that are responsible for the nucleosome structure of the chromosomal fibre in eukaryotes and have important regulatory functions dictated by their covalent modifications (Xu et al., 2009). Two molecules of each of the four core histones (H2A, H2B, H3, and H4) form an octamer, around which DNA is wrapped in repeating units, called nucleosomes. The linker histone, H1, interacts with linker DNA between nucleosomes and functions in the compaction of chromatin into higher order structures. Nucleosomes wrap and compact DNA, thereby limiting DNA accessibility to the cellular processes requiring DNA templates. Accordingly, histones play an essential role in transcription regulation, DNA replication, DNA repair, and chromosomal stability. Several of the histones detected in this study were up-regulated by 10 $\mu\text{g/mL}$ f-CNT exposures, and all were up-regulated by exposure to MWCNT-PVP at 500 pg/mL , including histone-lysine N-methyltransferase (MLL). In proliferating cells, histone expression is up-regulated at the onset of S phase (Osley, 1991). When DNA is damaged, its replication is suspended and histone transcription also ceases (Su et al., 2004). Pelka et al. (2011) recently showed that sodium cholate-dispersed SWCNTs were capable of generating ROS in HT29 cells exposed to 100 ng/mL for 3 h and causing DNA damage at exposures as low as 50 pg/mL , an effect not associated with any of the exposures in the current study. Our results suggest that these tightly regulated processes may be altered in some way by f-CNT exposure, perhaps through yet unexplained cellular metabolic signaling (Su et al., 2004).

By contrast, the possibility that the confluent cells in the Caco-2/HT29-MTX monolayer were actively or abnormally proliferating based on elevated histone expression seems unlikely as the cell proliferation assay (XTT analysis) showed no differences across the groups, and numerous components of the protein synthetic machinery were down-regulated. Eukaryotic translation initiation factor 3, subunits C and F along with 20 other eukaryotic translation initiation factors and 61 different ribosomal proteins were detected and compared, and generally all were down-regulated. In the MWCNT-PVP 500 pg/mL exposure, EIF3F and EIF3K were down-regulated while EEF1B2, EEF2, EIF3A, EIF3C,

EIF4A2, EIF4A3, EIF5, and 22 ribosomal proteins were up-regulated. Because down-regulation of ribosomal proteins commonly is associated with growth arrest, the contradiction between histone up-regulation and protein synthesis-associated protein down-regulation applies only to the 10 µg/mL f-CNT exposures and MWCNT-COOH at 500 pg/mL, and this remains to be clarified by additional investigation. The effect of MWCNT-PVP exposure at 500 pg/mL, where 97% of differentially expressed proteins were up-regulated, seems consistent with histone and protein synthesis machinery response. The unique, overall response to this exposure is discussed below.

Like the translation initiation factors above, gastric cancer-related protein (GCYS-20) was down-regulated by the f-CNT exposures. GCYS-20 is a 38.8 kDa protein whose gene sequence was originally obtained from a patient with glandular gastric cancer by LD-PCR based on subtractive hybridisation between gastric cancer and paracancer tissue (Cui et al., 2005). It frequently has been shown in microarray studies to be associated with other cancers, as well. The gene ontology database (Boyle et al., 2004) indicates a nucleic acid binding molecular function, and according to InterPro, GCYS-20 is characterised by a ribonuclease H-like domain, the catalytic domain of several polynucleotidyl transferases. A BLAST search of similar gene sequences identified several prokaryotic transposases. While its detection in the co-culture of two colorectal adenocarcinoma cell lines is not surprising, it is significant (two-fold) and consistent down-regulation by f-CNT exposure is interesting but difficult to interpret without considerable speculation.

4.3 Overall protein expression changes – functions, pathways, and networks

When overall differential protein expression was examined (Figure 7), a significantly lower number of proteins were affected by SWCNT-COOH exposure than either of the f-MWCNTs. Down-regulation of protein expression dominated most f-CNT exposures, though low-dose MWCNT-PVP exposure uniquely up-regulated 97% of the altered proteins, and it had the greatest effect on differential expression (256 proteins).

While analyses of ‘molecular and cellular functions’ or ‘canonical pathways’ are often useful in interpreting changes induced by differential protein expression in response to specific stimuli, we were unable to identify broadly consistent changes using these analyses with respect to f-CNT exposure. This may be consistent with the lack of overt toxicity and loss of cellular integrity we observed, and it suggests that these nanoparticles are likely to evoke very specific cellular responses depending on their physicochemical differences. Although differentially expressed proteins were significantly mapped to the generic pathways, functions, etc., it must be emphasised that the associated pathways are themselves rather complex with numerous protein components, most of which were unaffected by f-CNT exposure. Thus, to conclude that the exposures broadly altered these pathways would be speculative. What can be concluded is that the f-CNTs uniquely affected the culture system with little overlap between them.

At the 500 pg/mL exposure, SWCNT-COOH had little effect on protein expression and thus was not associated significantly with any molecular and cellular functions. By contrast, MWCNT-COOH and MWCNT-PVP exposures had significant effects and functional implications at this low dose. Both altered protein synthetic and cell death associated functions, but in opposing ways. Whereas MWCNT-COOH exposure down-regulated proteins associated with those two, it also uniquely and generally decreased those mapped to carbohydrate metabolism, cell movement, and energy production. In contrast, proteins altered by MWCNT-PVP exposure revealed increased protein synthetic and cell death associated functions, and uniquely increased post-translational modification, RNA post-transcriptional modification, and protein folding processes. These functional results, along

with a predominantly up-regulated proteome, suggest a stimulatory effect by MWCNT-PVP and an inhibitory effect of MWCNT-COOH at this extraordinarily low exposure level.

At the higher exposure level, functional effects of the two carboxylated CNTs demonstrated significant overlap, in terms of cell morphology, assembly, and organisation and protein synthesis. By contrast, MWCNT-PVP decreased function related to lipid metabolism, small molecule biochemistry, and energy production. In direct contrast to its effects at the low dose, MWCNT-PVP decreased RNA post-transcriptional modification function at 10 µg/mL.

With respect to canonical pathway analysis, the eukaryotic initiation factor 2 (EIF2) signalling pathway was altered by low-dose MWCNT-COOH (down-regulation) and MWCNT-PVP (up-regulation), and was the only canonical pathway common to these exposures at 500 µg/mL. At 10 µg/mL this pathway was common to all exposures, down-regulated by SWCNT-COOH and MWCNT-COOH, and up-regulated by MWCNT-PVP. In response to environmental stresses, a family of protein kinases phosphorylate EIF2 to alleviate cellular injury or alternatively induce apoptosis. Phosphorylation of EIF2 reduces global translation, allowing cells to conserve resources and to initiate a reconfiguration of gene expression to effectively manage stress conditions. Activation of EIF2 signalling pathway through component gene up-regulation is widely recognised as a key contributor to ER stress, such as that resulting from treatment with hepatotoxicants (Low et al., 2011).

We have previously observed unique patterns of differential protein expression in kidney barrier epithelia when unrefined, non-functionalised fullerenes, SWCNT, and MWCNT were compared (Blazer-Yost et al., 2011). One explanation for the unique cellular responses observed in the present study may be related to nanoparticle interactions with proteins in the fetal calf serum-supplemented culture media, whereby proteins adsorb to the nanoparticles to form a 'corona' that changes their physicochemical properties and dictates their bioactivity. Protein interaction with nanoparticles is rapid and dependent on surface properties and size (Zhang et al., 2011). The NP-protein complex and its 'epitope map' (Lynch et al., 2007) can be viewed as the biologically active entity to which the cells actually respond. Though the corona has been shown to reduce cytotoxicity, perhaps by decreased NP uptake by cells (Jiang et al., 2010; Casals et al., 2011; Ge et al., 2011; Safi et al., 2011) or by mitigating cell membrane damage (Hu et al., 2011), its unique constituency must be considered in assessing both *in vivo* and *in vitro* NP effects and when comparing the effects of various NPs with unique surface properties. Formation of protein coronas in the current study may account for the heterogeneity observed in f-CNT effects on protein expression, and this phenomenon is currently under investigation in our laboratory where we have observed unique protein composition for each CNT corona (unpublished).

4.4 Notable proteins whose expression was unaffected by f-CNT exposure

The expression of 1,854 of the 2,282 unique proteins detected and quantified in the present study remained unaltered after f-CNT exposure. It is important to consider some of those that may be related to the cytotoxicity indices that were unaffected by exposure, but have been previously observed to respond to CNT exposure in other cell culture models (Witzmann and Monteiro-Riviere, 2006; Rotoli et al., 2008; Coyuco et al., 2011; Teegarden et al., 2011). For example, with respect to tight junctional proteins, results of the Lucifer Yellow Assay were confirmed by a general lack of change in the expression of numerous proteins known to be closely associated with adhesional and cytoskeletal aspects of epithelial tight-junctions (Tang, 2006): junction protein ZO-2 (TJP2), actinin alpha 1 and 4, (ACTN1 and ACTN4), actin-related protein 2/3 complex subunit 2 (ARPC2), catenin alpha-1 (CTNNA1), catenin delta-1 (CTNND1), CD2-associated protein (CD2AP), desmoplakin (DSP), destrin (DST), ezrin (EZR), inactive tyrosine-protein kinase 7 (PTK7),

keratin-8 (KRT8), keratin-9 (KRT9), keratin-10 (KRT10), plakophilin-3 (PKP3), protein diaphanous homolog 1 (DIAPH1), protein enabled homolog (ENAH), spectrin alpha chain, brain 1 (SPTAN1), spectrin beta chain, brain 4 (SPTBN4), tropomyosin 3 (TPM3), and vinculin (VCL). In contrast, integrin alpha-6 (ITGA6) and poly(A) binding protein (PABPC1) were down-regulated by MWCNT-COOH at 10 µg/mL and LIM domain and actin-binding protein 1 (LIMA1), actinin, alpha 1 (ACTN1), ezrin (EZR), and tropomyosin 3 (TPM3) were up-regulated by MWCNT-PVP at 500 pg/mL.

No changes were observed in the expression of detoxification enzymes such as glutathione synthetase, glutathione S-transferase omega 1, glutathione S-transferase P, glutathione S-transferase kappa 1, glutathione S-transferase A1, glutathione S-transferase A3, mitochondrial phospholipid hydroperoxide glutathione peroxidase, peroxiredoxin (1, 2, 4, 5, and 6), and superoxide dismutase (Cu-Zn and Mn).

4.5 Considering exposure and dose

To approximate the number of particles in each exposure, we estimated the mass of the CNTs used in the study to be 3,888.3 g/mol/nm for SWCNT and 879,898.9 g/mol/nm for MWCNT. Ignoring the minor contribution of functionalisation to the CNT mass and using the exposure concentrations (with 1.5 mL added to the co-cultures), we further estimated that ~6.6 million single-walled tubes were contained in the 500 pg/mL exposure and 132.8 billion tubes comprised the 10 µg/mL dose. For the MWCNT, we estimated that the 500 pg/ml exposures contained ~0.2 million tubes while the 10 µg/mL dose contained 4.1 billion tubes. While we realise these are rough estimates, given the mass differences between the SW and MW nanotubes, the comparable concentrations actually reflect a ~32-fold greater SWCNT exposure than MWCNT. In view of these estimates, colloidal stability data, and the assumption that even at very low concentrations aggregation and bundling are likely, the SWCNT-COOH have comparatively little effect, compared to either f-MWCNT. Furthermore, given the fact that ~750,000 cells/Transwell™ insert were exposed to the f-CNTs, the relative number of nanotubes with the potential for interaction with the surface of the cell (or cell entry) is quite low. These considerations suggest the potential for individual f-CNT-mediated perturbation in this culture system may actually be quite high, particularly in view of the significant effects of the 500 pg/mL MWCNT-PVP exposure (~0.3 nanotubes/cell) and call into question the possibility of bystander effects similar to those observed in exposure to radiation (Blyth and Sykes, 2011) and polystyrene nanoparticles (Thubagere and Reinhard, 2010), particularly *in vitro*.

Another consideration that was not investigated is the effect of pH on the f-CNTs' physicochemical properties. To properly simulate *in vivo* f-CNT ingestion, regional exposure to differential pH environments must be taken into account. When nanoparticles are ingested *in vivo*, to reach the small intestine they must pass through an acidic gastric luminal environment (pH 1 to 3.5) followed by neutralisation in the small intestine. These environments can be expected to alter surface chemistry and cytotoxicity (Wang et al., 2008), particularly in nanoparticles where zeta potential is particularly dependent on pH (Loretz and Bernkop-Schnurch, 2007). *In vitro* studies simulating intestinal exposure should incorporate f-CNT treatment with simulated gastric fluid (SGF) and simulated intestinal fluid (SIF) prior to exposure, and they then should be characterised in the culture medium.

In view of the potential effect of GI tract pH extremes on surface charge and corona formation and the observed differential stability of the three f-CNTs in the culture media, additional studies to:

1. assess the effect of exposure to simulated gastric (SGF) and intestinal (SIF) fluids

2. determine actual f-CNT ‘cellular dose’ accompanying these exposures are currently underway.

5 Conclusions

The protein expression profiles presented here represent the first of their kind in *in vitro* nanotoxicology. The results are the first extensive proteomic description of biological responses to f-CNT in intestinal cells and, importantly, they describe non-cytotoxic mechanisms by which nanomaterials may influence cellular processes. Exposure to f-CNTs, even at very low levels, resulted in significant alterations in protein expression that were specific to f-CNT concentration and both nanotube type and functionalisation. These results suggest that acute and chronic exposure to ingested carbon nanoparticles, both *in vitro* and *in vivo*, even in the absence of overt toxicity, may have significant biological effects that should be evaluated more thoroughly, in view of the rapid development of novel fields of applications, increased production, and increased potential exposure of humans through accumulation along the food chain.

Supplementary Material

Refer to Web version on PubMed Central for supplementary material.

Acknowledgments

The authors gratefully acknowledge the technical assistance of Meixian Fang (Witzmann Lab) and Dr. Richard Day, Department of Cellular and Integrative Physiology, who obtained the bright field images. This study was supported in its entirety by NIH grants ES018810 and GM085218 (FAW).

Biographies

Xianyin Lai is an Assistant Research Professor at the Department of Cellular and Integrative Physiology, Indiana University School of Medicine. He received his PhD from Peking University, China. His research involves the application of proteomic techniques to investigate ‘molecular biomarkers’ and elucidate ‘molecular mechanisms’ in biomedical research. His experience relates to areas in proteomics, biomarkers, biochemistry, separation science, bioanalysis, HPLC, mass spectrometry, and analytical chemistry. He also has developed a label-free quantitative mass spectrometric software platform, IdentiQuantXL™.

Bonnie Blazer-Yost is a Professor at the Department of Biology, Indiana University – Purdue University Indianapolis with joint appointments at the Department of Integrative and Cellular Physiology and the Department of Anatomy and Cell Biology at the Indiana University School of Medicine. The main focus of her laboratory is the physiology and pathophysiology of barrier epithelial cells. Currently her group is investigating how various hormones regulate transepithelial ion transport in renal, airway and intestinal cells and how carbon nanotubes alter important components of the barrier function of these epithelial tissues.

James Clack studied Neurobiology at Purdue University and received his PhD in 1982. He then completed a postdoctoral fellowship at Yale University School of Medicine in 1984. He remained at Yale until 1990, and then moved to the Department of Biology and Indiana University – Purdue University Indianapolis. He is currently an Associate Professor of Biology and Head of the Purdue University Division of Science. His interests include the functional biochemistry of visual transduction/adaptation and the analysis of proteins as biomarkers for cellular and tissue injury precipitated by environmental stressors.

Sharry Fears studied Biochemistry at Purdue University, and worked in research for several years at an animal pharmaceutical company, Pitman-Moore, Inc. She continued her studies, earning a Master of Science in Biotechnology at Indiana University while teaching cell biology and proteomic techniques to graduate students who were enrolled in the Biotechnology Training Program. At IU, she acquired cell culture skills, including the co-culturing technique, and worked with several eukaryotic cell lines. She continues working in cell culture at Sensient Bio-Ingredients.

Somenath Mitra is a Distinguished Professor of Chemistry and Chair at the Department of Chemistry and Environmental Science at the New Jersey Institute of Technology. His current research focuses on nanotechnology, carbon nanotubes, energy applications such as solar cells and batteries, environmental remediation using nanosorbents and nanostructured membranes. His group has also developed a wide range of chemical sensors, instrumentation, as well as micro fabricated devices for real time environmental monitoring. He is the co-author/editor of two books, and has over 120 peer reviewed publications, and nearly 300 conference presentations. He received his BS in Chemical Engineering from Indian Institute of Technology and his PhD in Analytical Chemistry from Southern Illinois University in Carbondale, IL.

Susana Addo Ntim is a Research Associate at the Laboratory for Analytical Chemistry and Nanotechnology, Department of Chemistry and Environmental Science, New Jersey Institute of Technology, Newark, New Jersey. She recently graduated with a PhD in Environmental Science from the same university where she studied carbon nanotube functionalisation, applications and environmental implications. Her research spans areas in environmental science, nanotechnology, material characterisation, analytical chemistry and toxicology. She holds a Master of Science in Marine Estuarine Environmental Science from the University of Maryland Eastern Shore in Princess Anne Maryland and a Bachelor's degree in Chemistry from Kwame Nkrumah University of Science and Technology in Ghana.

Heather Ringham is a Research Technician at the Department of Cellular and Integrative Physiology, Indiana University for Dr. Frank Witzmann's group. In 2004, she earned a graduate certificate from the Biotechnology Research Training Program at Indiana University and a Master of Science degree in Biochemistry and Molecular Biology from Indiana University in 2009. She has been a member of Witzmann's research group since 2001 and is responsible for cell culture, nanoparticle exposure, cell-based assays, and mass spectrometry sample preparation.

Frank Witzmann is a Professor of Cellular and Integrative Physiology from Indiana University School of Medicine. He has applied proteomic analyses in a variety of paradigms since the mid-1980s (well before the term proteomics was coined) and currently directs the use of gel and mass spec-based proteomic approaches in projects ranging from various aspects of toxicology, pharmacology, vascular biology, and CNS physiology. He has published over 140 refereed manuscripts and book chapters, and is currently on the editorial board of *Analytical Biochemistry*.

References

- Amacher DE. The discovery and development of proteomic safety biomarkers for the detection of drug-induced liver toxicity. *Toxicol. Appl. Pharmacol.* 2010; Vol. 245(No. 1):134–142. [PubMed: 20219512]

- Arneson LS, Miller J. The chondroitin sulfate form of invariant chain trimerizes with conventional invariant chain and these complexes are rapidly transported from the trans-Golgi network to the cell surface. *Biochem. J.* 2007; Vol. 406(No. 1):97–103. [PubMed: 17492940]
- Banga A, Witzmann FA, et al. Functional effects of nanoparticle exposure on Calu-3 airway epithelial cells. *Cell Physiol. Biochem.* 2012; Vol. 29:197–212. [PubMed: 22415089]
- Blazer-Yost BL, Banga A, et al. Effect of carbon nanoparticles on renal epithelial cell structure, barrier function, and protein expression. *Nanotoxicology.* 2011; Vol. 5(No. 3):354–371. [PubMed: 21067278]
- Blazer-Yost BL, West TA, et al. Effect of the mycotoxin, ochratoxin A, on hormone-stimulated ion transport in a cultured cell model of the renal principal cell. *Pflugers Arch.* 2005; Vol. 450(No. 1): 53–60. [PubMed: 15630601]
- Blyth BJ, Sykes PJ. Radiation-induced bystander effects: what are they, and how relevant are they to human radiation exposures? *Radiat. Res.* 2011; Vol. 176(No. 2):139–157. [PubMed: 21631286]
- Borm P, Klaessig FC, et al. Research strategies for safety evaluation of nanomaterials, part V: role of dissolution in biological fate and effects of nanoscale particles. *Toxicol. Sci.* 2006; Vol. 90(No. 1): 23–32. [PubMed: 16396841]
- Borm PJ, Robbins D, et al. The potential risks of nanomaterials: a review carried out for ECETOC. *Part Fibre Toxicol.* 2006; Vol. 3:11–45. [PubMed: 16907977]
- Boyle EI, Weng SA, et al. GO::TermFinder - open source software for accessing gene ontology information and finding significantly enriched gene ontology terms associated with a list of genes. *Bioinformatics.* 2004; Vol. 20(No. 18):3710–3715. [PubMed: 15297299]
- Byrd JC, Bresalier RS. Mucins and mucin binding proteins in colorectal cancer. *Cancer Metastasis Rev.* 2004; Vol. 23(Nos. 1-2):77–99. [PubMed: 15000151]
- Calnek D, Quaroni A. Differential localization by in situ hybridization of distinct keratin mRNA species during intestinal epithelial cell development and differentiation. *Differentiation.* 1993; Vol. 53(No. 2):95–104. [PubMed: 7689500]
- Casals E, Pfaller T, et al. Hardening of the nanoparticle-protein corona in metal (Au, Ag) and oxide (Fe(3) O(4) CoO, and CeO(2)) nanoparticles. *Small.* 2011; Vol. 7(No. 24):3479–3486. [PubMed: 22058075]
- Cha MH, Rhim T, et al. Proteomic identification of macrophage migration-inhibitory factor upon exposure to TiO₂ particles. *Mol. Cell Proteomics.* 2007; Vol. 6(No. 1):56–63. [PubMed: 17028300]
- Chen XM, Elisia I, et al. Defining conditions for the co-culture of Caco-2 and HT29-MTX cells using Taguchi design. *J. Pharmacol. Toxicol. Methods.* 2010; Vol. 61(No. 3):334–342. [PubMed: 20159047]
- Chen Y, Mitra S. Fast microwave-assisted purification, functionalization and dispersion of multi-walled carbon nanotubes. *Journal of Nanoscience and Nanotechnology.* 2008; Vol. 8:5770–5775. [PubMed: 19198303]
- Chen Y, Iqbal Z, et al. Microwave-induced controlled purification of single-walled carbon nanotubes without sidewall functionalization. *Advanced Functional Materials.* 2007; Vol. 17(No. 18):3946–3951.
- Chiu KH, Lee WL, et al. A label-free differential proteomic analysis of mouse bronchoalveolar lavage fluid exposed to ultrafine carbon black. *Anal. Chim. Acta.* 2010; Vol. 673(No. 2):160–166. [PubMed: 20599030]
- Chu P, Wu E, et al. Cytokeratin 7 and cytokeratin 20 expression in epithelial neoplasms: a survey of 435 cases. *Mod. Pathol.* 2000; Vol. 13(No. 9):962–972. [PubMed: 11007036]
- Coyuco JC, Liu Y, et al. Functionalized carbon nanomaterials: exploring the interactions with Caco-2 cells for potential oral drug delivery. *International Journal of Nanomedicine.* 2011; Vol. 6(No. 1): 2253–2263. [PubMed: 22125408]
- Cui DX, Zhang L, et al. A microarray-based gastric carcinoma prewarning system. *World J. Gastroenterol.* 2005; Vol. 11(No. 9):1273–1282. [PubMed: 15761963]
- Donaldson K, Aitken R, et al. Carbon nanotubes: a review of their properties in relation to pulmonary toxicology and workplace safety. *Toxicol. Sci.* 2006; Vol. 92(No. 1):5–22. [PubMed: 16484287]

- Edgar R, Domrachev M, et al. Gene expression omnibus: NCBI gene expression and hybridization array data repository. *Nucleic Acids Research*. 2002; Vol. 30(No. 1):207–210. [PubMed: 11752295]
- Folkmann JK, Risom L, et al. Oxidatively damaged DNA in rats exposed by oral gavage to C60 fullerenes and single-walled carbon nanotubes. *Environ. Health Perspect*. 2009; Vol. 117(No. 5): 703–708. [PubMed: 19479010]
- Ge C, Du J, et al. Binding of blood proteins to carbon nanotubes reduces cytotoxicity. *Proc. Natl. Acad. Sci. USA*. 2011; Vol. 108(No. 41):16968–16973. [PubMed: 21969544]
- Grieb G, Merk M, et al. Macrophage migration inhibitory factor (MIF): a promising biomarker. *Drug News Perspect*. 2010; Vol. 23(No. 4):257–264. [PubMed: 20520854]
- Hardwidge PR, Rodriguez-Escudero I, et al. Proteomic analysis of the intestinal epithelial cell response to enteropathogenic *Escherichia coli*. *Journal of Biological Chemistry*. 2004; Vol. 279(No. 19):20127–20136. [PubMed: 14988394]
- Helsens K, Martens L, et al. Mass spectrometry-driven proteomics: an introduction. *Methods Mol. Biol*. 2011; Vol. 753:1–27. [PubMed: 21604112]
- Hilgendorf C, Spahn-Langguth H, et al. Caco-2 versus Caco-2/HT29-MTX co-cultured cell lines: permeabilities via diffusion, inside- and outside-directed carrier-mediated transport. *J. Pharm. Sci*. 2000; Vol. 89(No. 1):63–75. [PubMed: 10664539]
- Hu W, Peng C, et al. Protein corona-mediated mitigation of cytotoxicity of graphene oxide. *ACS Nano*. 2011; Vol. 5(No. 5):3693–3700. [PubMed: 21500856]
- Ito Y, Venkatesan N, et al. Effect of fiber length of carbon nanotubes on the absorption of erythropoietin from rat small intestine. *IntJPharm*. 2007; Vol. 337(Nos. 1-2):357–360.
- Jiang X, Weise S, et al. Quantitative analysis of the protein corona on FePt nanoparticles formed by transferrin binding. *Journal of The Royal Society Interface*. 2010; Vol. 7(Supplement 1):S5–S13.
- Johansson ME, Thomsson KA, et al. Proteomic analyses of the two mucus layers of the colon barrier reveal that their main component, the Muc2 mucin, is strongly bound to the Fcgbp protein. *J. Proteome Res*. 2009; Vol. 8(No. 7):3549–3557. [PubMed: 19432394]
- Johnston HJ, Hutchison GR, et al. A critical review of the biological mechanisms underlying the in vivo and in vitro toxicity of carbon nanotubes: the contribution of physico-chemical characteristics. *Nanotoxicology*. 2010; Vol. 4(No. 2):207–246. [PubMed: 20795897]
- Jos A, Pichardo S, et al. Cytotoxicity of carboxylic acid functionalized single wall carbon nanotubes on the human intestinal cell line Caco-2. *Toxicol. in Vitro*. 2009; Vol. 23(No. 8):1491–1496. [PubMed: 19591917]
- Kateb B, Van Handel M, et al. Internalization of MWCNTs by microglia: possible application in immunotherapy of brain tumors. *NeuroImage*. 2007; Vol. 37(Supplement 1):S9–S17. [PubMed: 17601750]
- Keller A, Nesvizhskii AI, et al. Empirical statistical model to estimate the accuracy of peptide identifications made by MS/MS and database search. *Anal. Chem*. 2002; Vol. 74(No. 20):5383–5392. [PubMed: 12403597]
- Kennedy AJ, Hull MS, et al. Factors influencing the partitioning and toxicity of nanotubes in the aquatic environment. *Environ. Toxicol. Chem*. 2008; Vol. 27(No. 9):1932–1941. [PubMed: 19086318]
- Koeneman BA, Zhang Y, et al. Experimental approach for an in vitro toxicity assay with non-aggregated quantum dots. *Toxicology in Vitro*. 2009; Vol. 23(No. 5):955–962. [PubMed: 19465109]
- Kolosnjaj-Tabi J, Hartman KB, et al. In vivo behavior of large doses of ultrashort and full-length single-walled carbon nanotubes after oral and intraperitoneal administration to Swiss mice. *ACS Nano*. 2010; Vol. 4(No. 3):1481–1492. [PubMed: 20175510]
- Krug HF, Wick P. *Nanotoxicology: an interdisciplinary challenge*. *Angewandte Chemie International Edition*. 2011; Vol. 50(No. 6):1260–1278.
- Kulamarva A, Bhathena J, et al. In vitro cytotoxicity of functionalized single walled carbon nanotubes for targeted gene delivery applications. *Nanotoxicology*. 2008; Vol. 2(No. 4):184–188.
- Kyu Kim H, Thu VT, et al. Cardiac proteomic responses to ischemia-reperfusion injury and ischemic preconditioning. *Expert Rev. Proteomics*. 2011; Vol. 8(No. 2):241–261.

- Lai X, Bacallao RL, et al. Characterization of the renal cyst fluid proteome in autosomal dominant polycystic kidney disease (ADPKD) patients. *Proteomics Clin. Appl.* 2008; Vol. 2(Nos. 7-8): 1140–1152. [PubMed: 20411046]
- Lai X, Wang L, et al. A novel alignment method and multiple filters for exclusion of unqualified peptides to enhance label-free quantification using peptide intensity in LC-MS/MS. *J. Proteome Res.* 2011; Vol. 10(No. 10):4799–4812. [PubMed: 21888428]
- Lam CW, James JT, et al. A review of carbon nanotube toxicity and assessment of potential occupational and environmental health risks. *Crit. Rev. Toxicol.* 2006; Vol. 36(No. 3):189–217. [PubMed: 16686422]
- Lesuffleur T, Barbat A, et al. Dihydrofolate reductase gene amplification-associated shift of differentiation in methotrexate-adapted HT-29 cells. *J. Cell Biol.* 1991; Vol. 115(No. 5):1409–1418. [PubMed: 1955481]
- Lesuffleur T, Porchet N, et al. Differential expression of the human mucin genes MUC1 to MUC5 in relation to growth and differentiation of different mucus-secreting HT-29 cell subpopulations. *J. Cell Sci.* 1993; Vol. 106(Pt. 3):771–783. [PubMed: 8308060]
- Li Y, Martin LD, et al. MARCKS protein is a key molecule regulating mucin secretion by human airway epithelial cells in vitro. *J. Biol. Chem.* 2001; Vol. 276(No. 44):40982–40990. [PubMed: 11533058]
- Loretz B, Bernkop-Schnurch A. In vitro cytotoxicity testing of non-thiolated and thiolated chitosan nanoparticles for oral gene delivery. *Nanotoxicology.* 2007; Vol. 1(No. 2):139–148.
- Low Y, Uehara T, et al. Predicting drug-induced hepatotoxicity using QSAR and toxicogenomics approaches. *Chemical Research in Toxicology.* 2011; Vol. 24(No. 8):1251–1262. [PubMed: 21699217]
- Lynch I, Cedervall T, et al. The nanoparticle - protein complex as a biological entity; a complex fluids and surface science challenge for the 21st century. *Advances in Colloid and Interface Science.* 2007; Vols. 134-135:167–174. [PubMed: 17574200]
- Maaser C, Eckmann L, et al. Ubiquitous production of macrophage migration inhibitory factor by human gastric and intestinal epithelium. *Gastroenterology.* 2002; Vol. 122(No. 3):667–680. [PubMed: 11875000]
- Mahler GJ, Esch MB, et al. Characterization of a gastrointestinal tract microscale cell culture analog used to predict drug toxicity. *Biotechnol. Bioeng.* 2009a; Vol. 104(No. 1):193–205. [PubMed: 19418562]
- Mahler GJ, Shuler ML, et al. Characterization of Caco-2 and HT29-MTX cocultures in an in vitro digestion/cell culture model used to predict iron bioavailability. *J. Nutr. Biochem.* 2009b; Vol. 20(No. 7):494–502. [PubMed: 18715773]
- Man AL, Lodi F, et al. Macrophage migration inhibitory factor plays a role in the regulation of microfold (M) cell-mediated transport in the gut. *J. Immunol.* 2008; Vol. 181(No. 8):5673–5680. [PubMed: 18832726]
- Maynard AD, Baron PA, et al. Exposure to carbon nanotube material: aerosol release during the handling of unrefined single-walled carbon nanotube material. *J. Toxicol. Environ. Health A.* 2004; Vol. 67(No. 1):87–107. [PubMed: 14668113]
- Miller C, Wang L, et al. The interplay between SUCLA2, SUCLG2, and mitochondrial DNA depletion. *Biochim. Biophys. Acta.* 2011; Vol. 1812(No. 5):625–629. [PubMed: 21295139]
- Monroe ME, Shaw JL, et al. MASIC: a software program for fast quantitation and flexible visualization of chromatographic profiles from detected LC-MS(/MS) features. *Comput. Biol. Chem.* 2008; Vol. 32(No. 3):215–217. [PubMed: 18440872]
- Mrsny RJ. Lessons from nature: 'pathogen-mimetic' systems for mucosal nano-medicines. *Adv. Drug Deliv. Rev.* 2009; Vol. 61(No. 2):172–192. [PubMed: 19146895]
- Nahar M, Dutta T, et al. Functional polymeric nanoparticles: an efficient and promising tool for active delivery of bioactives. *Crit. Rev. Ther. Drug Carrier Syst.* 2006; Vol. 23(No. 4):259–318. [PubMed: 17341200]
- Nanni P, Mezzanotte L, et al. Differential proteomic analysis of HT29 Cl.16E and intestinal epithelial cells by LC ESI/QTOF mass spectrometry. *Journal of Proteomics.* 2009; Vol. 72(No. 5):865–873. [PubMed: 19168159]

- Neilson KA, Ali NA, et al. Less label, more free: approaches in label-free quantitative mass spectrometry. *Proteomics*. 2011; Vol. 11(No. 4):535–553. [PubMed: 21243637]
- Nel A, Xia T, et al. Toxic potential of materials at the nanolevel. *Science*. 2006; Vol. 311(No. 5761): 622–627. [PubMed: 16456071]
- Nesvizhskii AI, Keller A, et al. A statistical model for identifying proteins by tandem mass spectrometry. *Anal. Chem*. 2003; Vol. 75(No. 17):4646–4658. [PubMed: 14632076]
- Ntim SA, Sae-Khow O, et al. Effects of polymer wrapping and covalent functionalization on the stability of MWCNT in aqueous dispersions. *Journal of Colloid and Interface Science*. 2011; Vol. 355:383–388. [PubMed: 21236442]
- Oberdorster G, Maynard A, et al. Principles for characterizing the potential human health effects from exposure to nanomaterials: elements of a screening strategy. *Particle and Fibre Toxicology*. 2005; Vol. 2(No. 1):8–43. [PubMed: 16209704]
- Osley MA. The regulation of histone synthesis in the cell cycle. *Annu. Rev. Biochem*. 1991; Vol. 60:827–861. [PubMed: 1883210]
- Osman AM, van Dartel DA, et al. Proteome profiling of mouse embryonic stem cells to define markers for cell differentiation and embryotoxicity. *Reprod. Toxicol*. 2010; Vol. 30(No. 2):322–332. [PubMed: 20553848]
- Park SW, Zhen G, et al. The protein disulfide isomerase AGR2 is essential for production of intestinal mucus. *Proc. Natl. Acad. Sci. USA*. 2009; Vol. 106(No. 17):6950–6955. [PubMed: 19359471]
- Pelka J, Gehrke H, et al. DNA damaging properties of single walled carbon nanotubes in human colon carcinoma cells. *Nanotoxicology*. 2011:1–19. (Epub ahead of print).
- Piovesan S, Cox PA, et al. Novel biocompatible chitosan decorated single-walled carbon nanotubes (SWNTs) for biomedical applications: theoretical and experimental investigations. *Phys. Chem. Chem. Phys*. 2010; Vol. 12(No. 48):15636–15643. [PubMed: 20589282]
- Ponti J, Colognato R, et al. Colony forming efficiency and microscopy analysis of multi-wall carbon nanotubes cell interaction. *Toxicology Letters*. 2010; Vol. 197(No. 1):29–37. [PubMed: 20435104]
- Robinson MS, Bonifacino JS. Adaptor-related proteins. *Curr. Opin. Cell Biol*. 2001; Vol. 13(No. 4): 444–453. [PubMed: 11454451]
- Rost M, Döring T, et al. 2-adaptin, a ubiquitin-interacting adaptor, is a substrate to coupled ubiquitination by the ubiquitin ligase Nedd4 and functions in the endosomal pathway. *Journal of Biological Chemistry*. 2008; Vol. 283(No. 46):32119–32130. [PubMed: 18772139]
- Rotoli BM, Bussolati O, et al. Non-functionalized multi-walled carbon nanotubes alter the paracellular permeability of human airway epithelial cells. *Tox. Lett*. 2008; Vol. 178(No. 2):95–102.
- Safi M, Courtois J, et al. The effects of aggregation and protein corona on the cellular internalization of iron oxide nanoparticles. *Biomaterials*. 2011; Vol. 32(No. 35):9353–9363. [PubMed: 21911254]
- Sari Y, Zhang M, et al. Differential expression of proteins in fetal brains of alcohol-treated prenatally C57BL/6 mice: a proteomic investigation. *Electrophoresis*. 2010; Vol. 31(No. 3):483–496. [PubMed: 20119957]
- Shane MA, Nofziger C, et al. Hormonal regulation of the epithelial Na⁺ channel: from amphibians to mammals. *Gen. Comp. Endocrinol*. 2006; Vol. 147(No. 1):85–92. [PubMed: 16405890]
- Simeonova PP. Update on carbon nanotube toxicity. *Nanomed*. 2009; Vol. 4(No. 4):373–375.
- Storey JD. A direct approach to false discovery rates. *Journal of the Royal Statistical Society Series B-Statistical Methodology*. 2002; Vol. 64:479–498.
- Su C, Gao G, et al. DNA damage induces down-regulation of histone gene expression through the G1 checkpoint pathway. *EMBO. J*. 2004; Vol. 23(No. 5):1133–1143. [PubMed: 14976556]
- Tang V. Proteomic and bioinformatic analysis of epithelial tight junction reveals an unexpected cluster of synaptic molecules. *Biology Direct*. 2006; Vol. 1(No. 1):1–37.
- Teeguarden JG, Webb-Robertson BJ, et al. Comparative proteomics and pulmonary toxicity of instilled single-walled carbon nanotubes, crocidolite asbestos, and ultrafine carbon black in mice. *Toxicol. Sci*. 2011; Vol. 120(No. 1):123–135. [PubMed: 21135415]

- Thubagere A, Reinhard BM. Nanoparticle-induced apoptosis propagates through hydrogen-peroxide-mediated bystander killing: insights from a human intestinal epithelium in vitro model. *ACS Nano*. 2010; Vol. 4(No. 7):3611–3622. [PubMed: 20560658]
- Veenstra TD. Proteomics research in breast cancer: balancing discovery and hypothesis-driven studies. *Expert Review of Proteomics*. 2011; Vol. 8(No. 2):139–141. [PubMed: 21501004]
- Veetil JV, Ye K. Development of immunosensors using carbon nanotubes. *Biotechnol. Prog.* 2007; Vol. 23(No. 3):517–531. [PubMed: 17458980]
- Veetil JV, Ye K. Tailored carbon nanotubes for tissue engineering applications. *Biotechnol. Prog.* 2009; Vol. 25(No. 3):709–721. [PubMed: 19496152]
- Walter E, Janich S, et al. HT29-MTX/Caco-2 cocultures as an in vitro model for the intestinal epithelium: in vitro-in vivo correlation with permeability data from rats and humans. *J. Pharm. Sci.* 1996; Vol. 85(No. 10):1070–1076. [PubMed: 8897273]
- Wang L, Nagesha DK, et al. Toxicity of CdSe nanoparticles in Caco-2 cell cultures. *J. Nanobiotechnology*. 2008; Vol. 6:11. [PubMed: 18947410]
- Wang X, Xia T, et al. Quantitative techniques for assessing and controlling the dispersion and biological effects of multiwalled carbon nanotubes in mammalian tissue culture cells. *ACS Nano*. 2010; Vol. 4(No. 12):7241–7252. [PubMed: 21067152]
- Wang Y, Iqbal Z, et al. Microwave-induced rapid chemical functionalization of single-walled carbon nanotubes. *Carbon*. 2005; Vol. 43(No. 5):1015–1020.
- Witzmann FA, Monteiro-Riviere NA. Multi-walled carbon nanotube exposure alters protein expression in human keratinocytes. *Nanomedicine*. 2006; Vol. 2(No. 3):158–168. [PubMed: 17292138]
- Worle-Knirsch JM, Pulskamp K, et al. Oops they did it again! Carbon nanotubes hoax scientists in viability assays. *Nano Lett.* 2006; Vol. 6(No. 6):1261–1268. [PubMed: 16771591]
- Xu D, Bai J, et al. Covalent modifications of histones during mitosis and meiosis. *Cell Cycle*. 2009; Vol. 8(No. 22):3688–3694. [PubMed: 19855177]
- Yao K, Shida S, et al. Macrophage migration inhibitory factor is a determinant of hypoxia-induced apoptosis in colon cancer cell lines. *Clinical Cancer Research*. 2005; Vol. 11(No. 20):7264–7272. [PubMed: 16243796]
- Zhang B, Chen Q, et al. Characterization of and biomolecule immobilization on the biocompatible multi-walled carbon nanotubes generated by functionalization with polyamidoamine dendrimers. *Colloids Surf B Biointerfaces*. 2010a; Vol. 80(No. 1):18–25. [PubMed: 20542415]
- Zhang X, Hui Z, et al. Alginate microsphere filled with carbon nanotube as drug carrier. *IntJBiol. Macromol.* 2010b; Vol. 47(No. 3):389–395.
- Zhang H, Burnum KE, et al. Quantitative proteomics analysis of adsorbed plasma proteins classifies nanoparticles with different surface properties and size. *Proteomics*. 2011; Vol. 11(No. 23):4569–4577. [PubMed: 21956884]
- Zhang T, Xu M, et al. Synthesis, characterization and cytotoxicity of phosphoryl cholinegrafted water-soluble carbon nanotubes. *Carbon*. 2008; Vol. 46(No. 13):1782–1791.

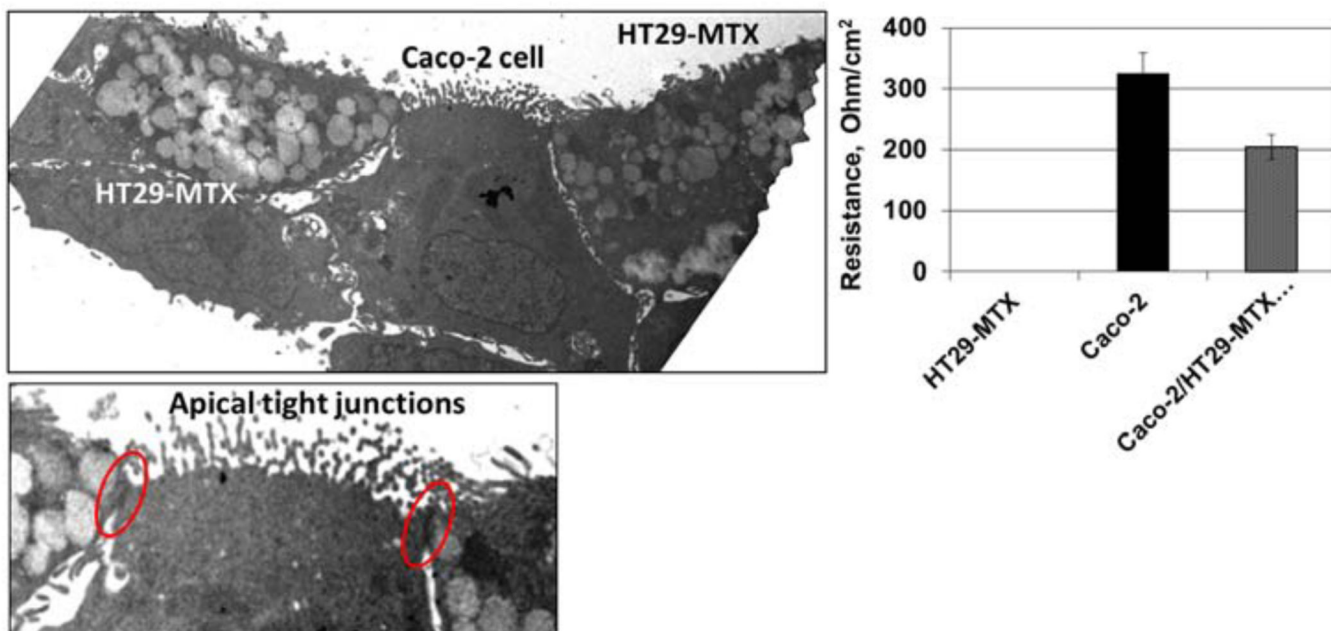


Figure 1.

Transmission electron micrographs of the Caco-2/HT29-MTX co-culture (at 14 d incubation) used in this study (see online version for colours)

Notes: The abundance of mucus-filled vesicles in the HT29-MTX cells and the development of prominent apical tight junctions. These morphological features are substantiated by the graphical representation of TEER measurements on the right.

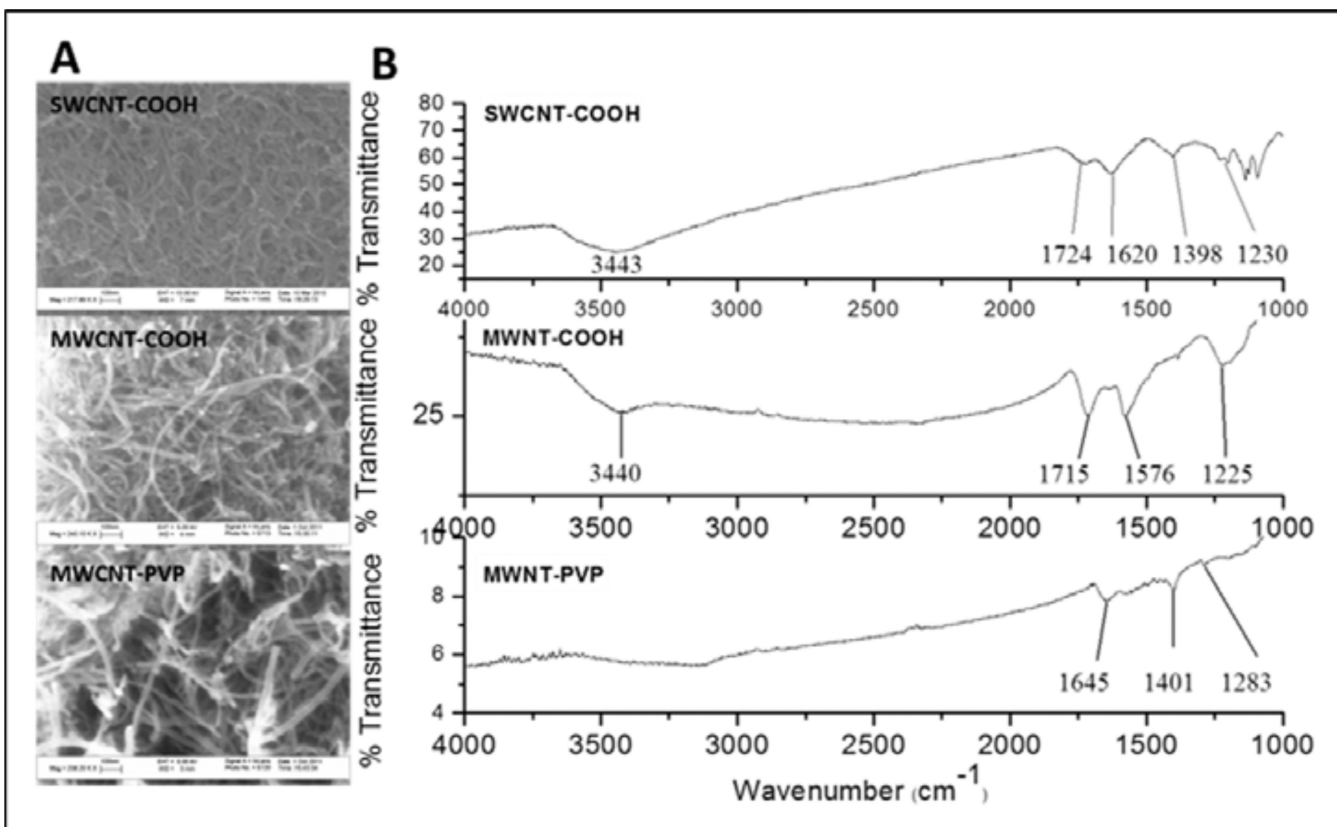


Figure 2.

(a) SEM and (b) FTIR spectroscopy results

Notes: The SEM images show that the tubes remained intact after acid treatment with minimal visible tube damage [Figure 2(a)]. It is apparent from the SEM images of MWCNT-PVP that the PVP was uniformly distributed on the nanotubes and the latter retained its morphology. The FTIR spectrum shown in Figure 2(b), confirmed the presence of functional groups in the f-CNTs.

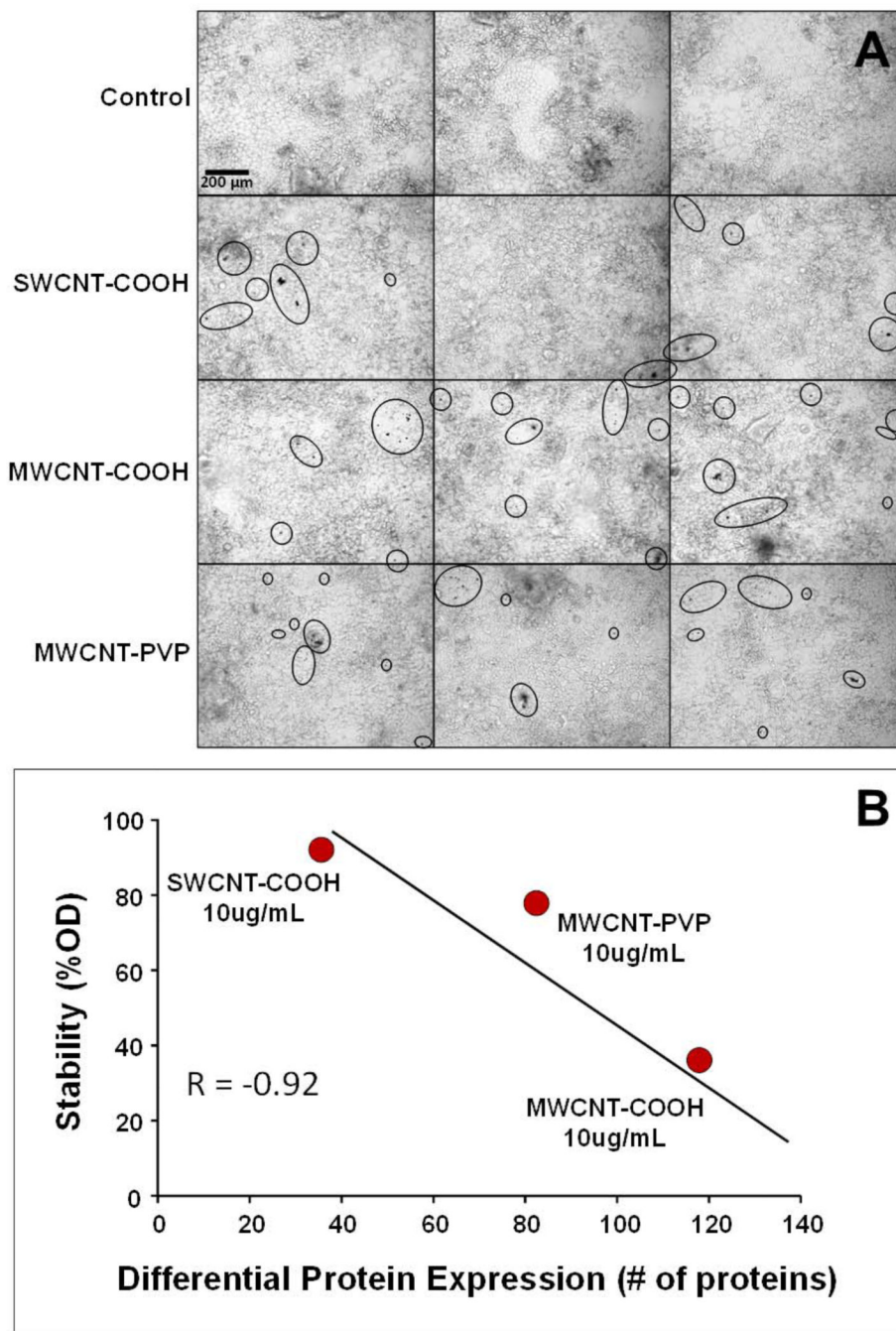


Figure 3.

(a) Bright field photomicrographs of triplicate, fully differentiated Caco-2/HT29-MTX co-cultures exposed to various f-CNTs at 10 µg/mL for 48 h* (b) Relationship between colloidal stability of the f-CNTs (10 µg/mL) in cell culture media and the number of proteins that were differentially expressed at that exposure** (see online version for colours)

Notes: *Circles emphasise aggregate formation via agglomeration, bundling, and entanglement of f-CNTs at the cell monolayer surface. **It is assumed that nanoparticle settling is a function of low stability.

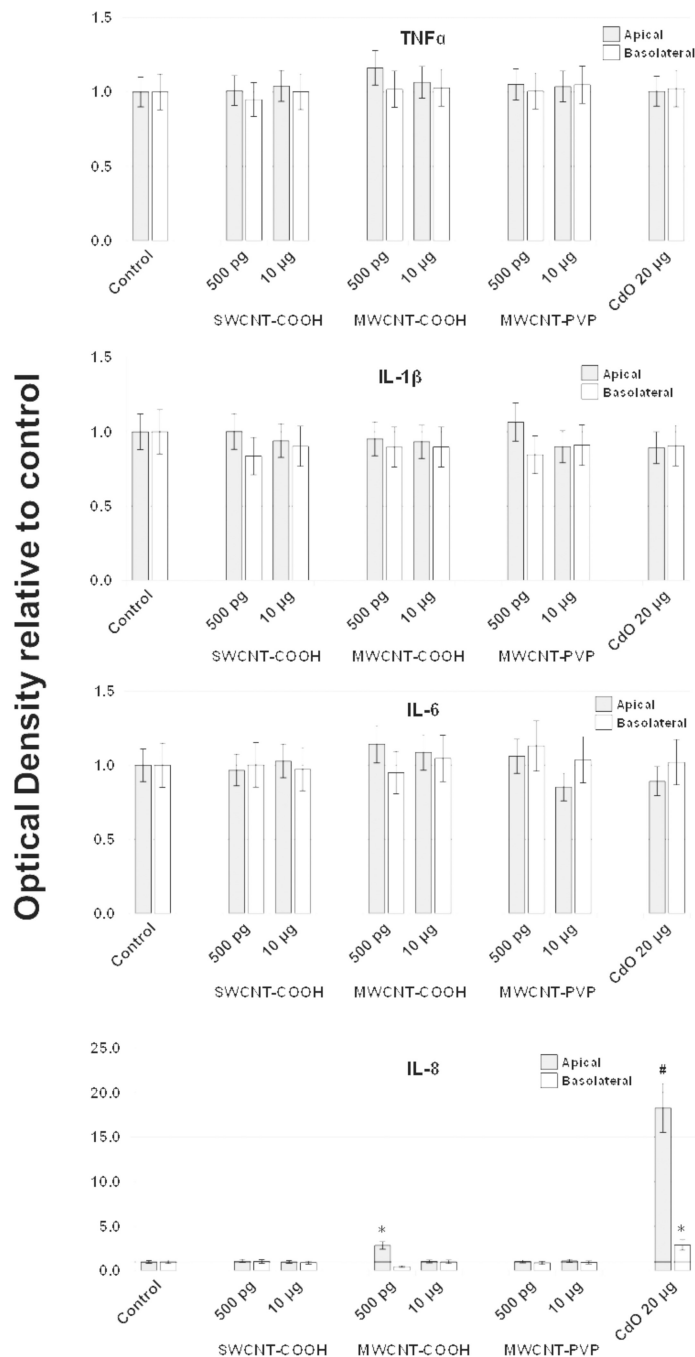
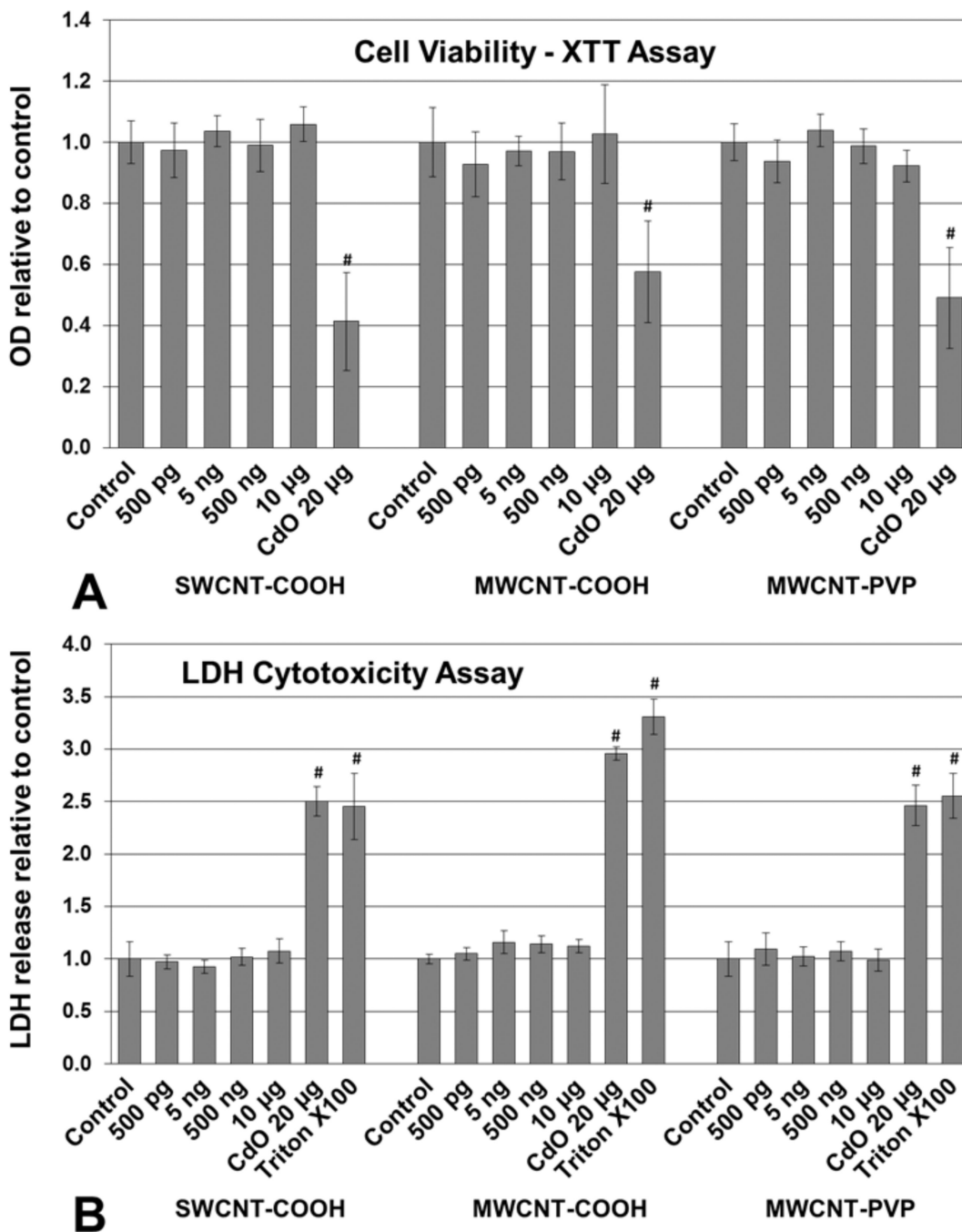


Figure 4.

Effect of f-CNT exposure on apical and basolateral secretion of cytokines by the Caco-2/HT29-MTX culture system after 48 h, determined by ELISA. CdO was included as a positive control at 20 μ g/mL

Notes: Values are means \pm SD for $n = 5$ with optical densities normalised to control. For IL-8, $p < 0.001$ for apical and basolateral measurements; *post hoc Holm-Sidak $p < 0.001$ vs. Control; #post hoc Holm-Sidak $p < 0.001$ vs. all others. All other cytokine comparisons were not statistically significant.



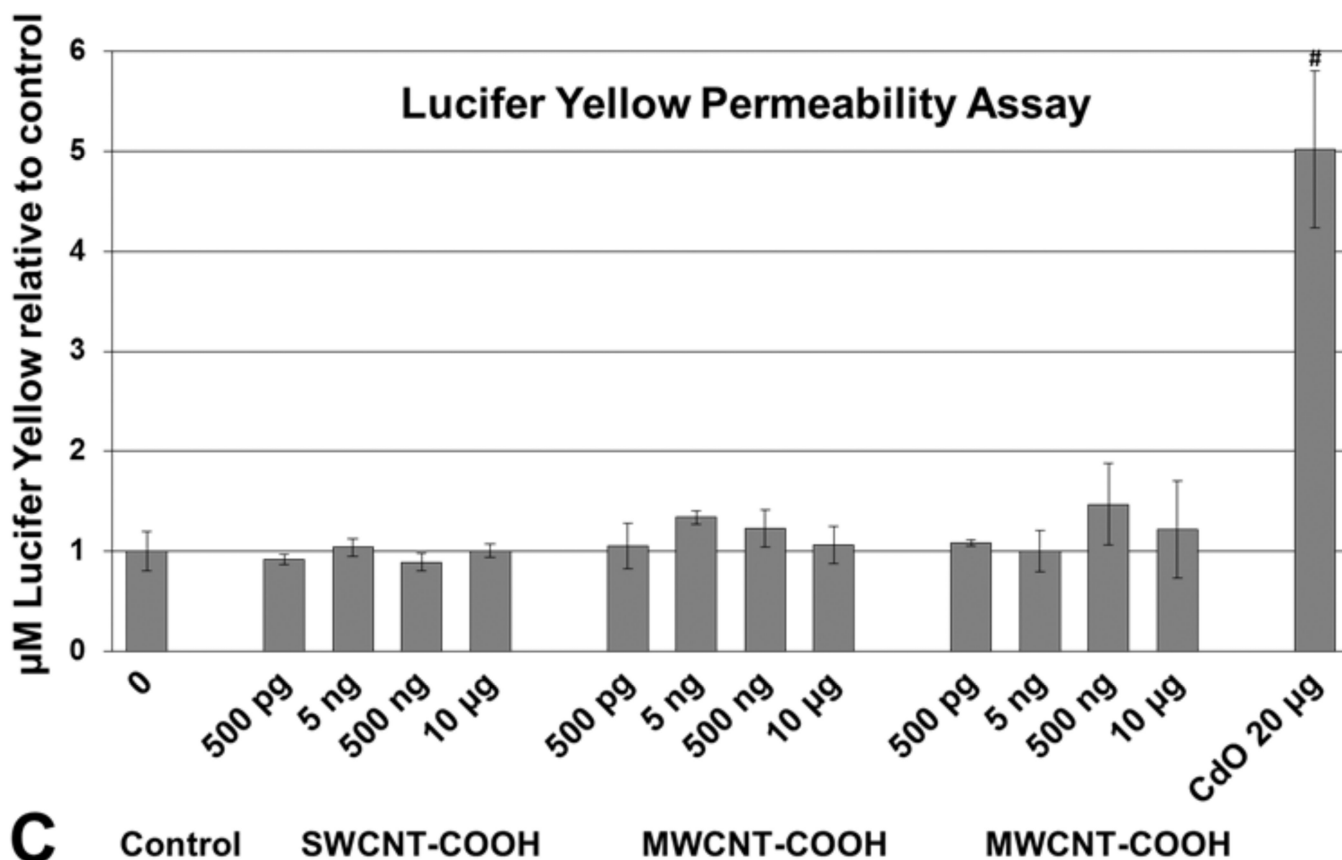


Figure 5.

Effect of f-CNT exposure on Caco-2/HT29-MTX: (a) cell viability after 48 h determined by XTT assay. CdO was included as a positive control at 20 µg/mL* (b) membrane integrity (LDH leakage) after 48 h determined by CytoTox 96 assay. Triton X100 and CdO were included as a positive controls** (c) epithelial barrier integrity (apical to basolateral compartment paracellular permeability) after 48 h determined by Lucifer Yellow assay***

Notes: *Values are means \pm SD for n=5 with optical densities normalised to control. ANOVA $p < 0.001$, #post hoc Holm-Sidak $p < 0.001$ vs. all others. **Values are means \pm SD for n = 5 with optical densities normalised to control. ANOVA $p < 0.001$, #post hoc Holm-Sidak $p < 0.001$ vs. all f-CNT treatments and control. ***Values are means \pm SD for n = 5 with LY concentration normalised to control. ANOVA $p < 0.001$, #post hoc Holm-Sidak $p < 0.001$ vs. all others.

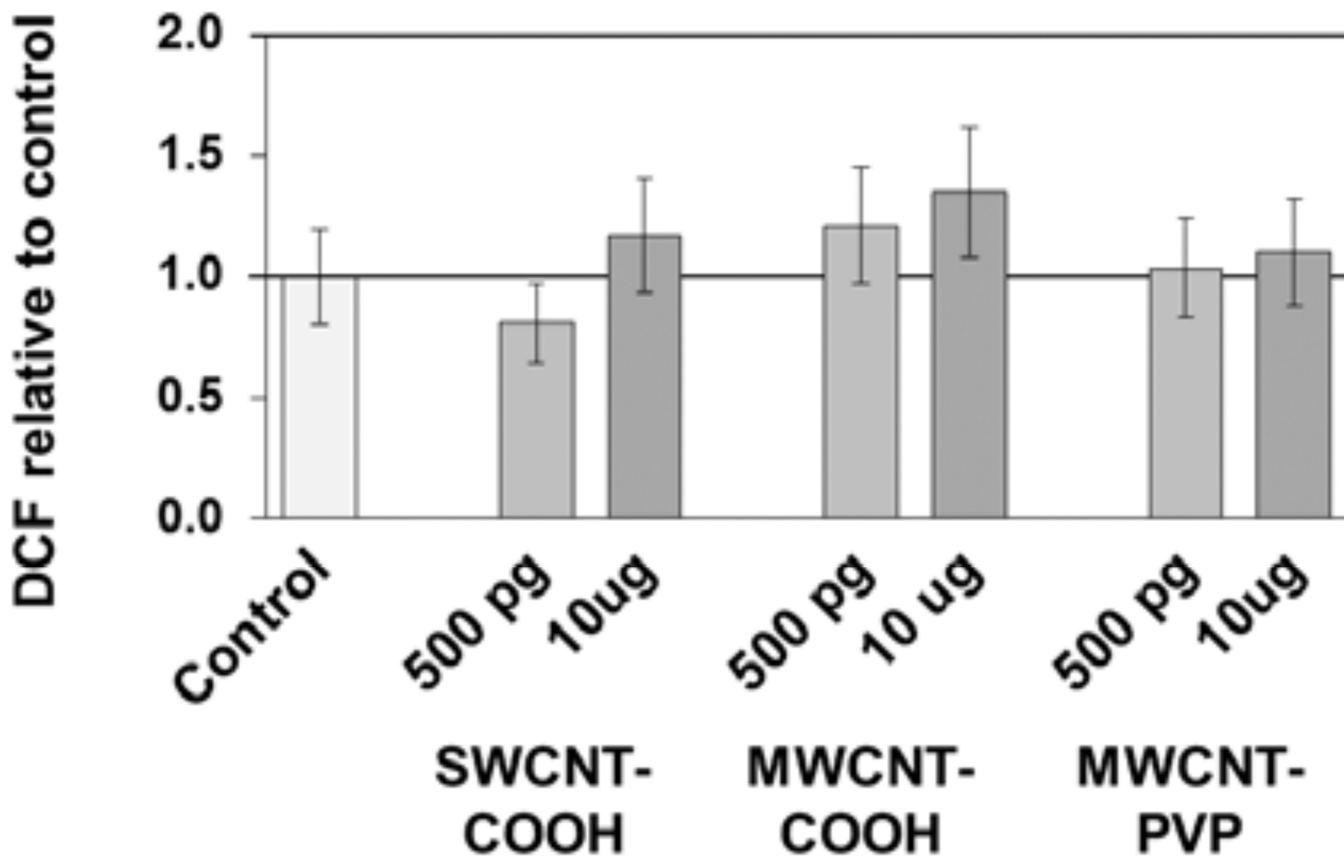


Figure 6. ROS formation in co-cultures after exposure to f-CNTs for 48 h, measured using the OxiSelect ROS assay

Notes: ROS generation is expressed as 2',7'-dichlorofluorescein (DCF) fluorescence normalised to the control. Values are means \pm SD for $n = 5$; ANOVA indicated no significant differences.

Number of differentially expressed proteins in Caco-2 /HT29-MTX co-cultures exposed to functionalized carbon nanotubes

f-CNT	500 pg/mL	10 µg/mL
SWCNT-COOH	13	33
MWCNT-COOH	109	118
MWCNT-PVP	256	83

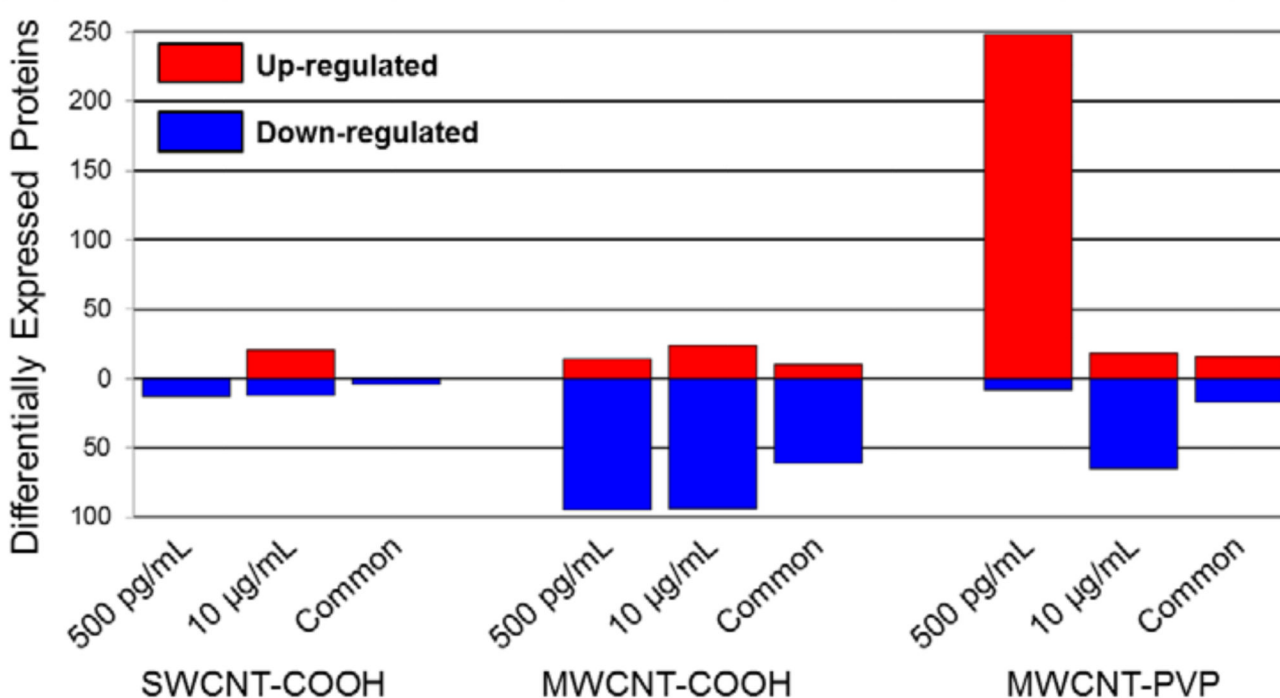


Figure 7.

Effect of f-CNT exposure on protein expression in Caco-2/HT29-MTX co-cultures (see online version for colours)

Notes: The top portion of the figure lists the number of proteins differentially expressed (ANOVA $p < 0.01$, $p < 0.05$ after Holm-Sidak multiple comparisons) by each exposure and nanoparticle from a total of 2,282 cellular proteins identified and quantified. These data are expanded in the graph, which illustrates the comparative extent of up- and down-regulation of the altered proteins. Overall, a significantly smaller number of proteins were affected by SWCNT-COOH exposure than either of the f-MWCNTs. Down-regulation of protein expression dominated most f-CNT exposures, though low-dose MWCNT-PVP exposure uniquely up-regulated 97% of the altered proteins, and it had the greatest effect of all f-CNTs on differential expression (256 proteins).

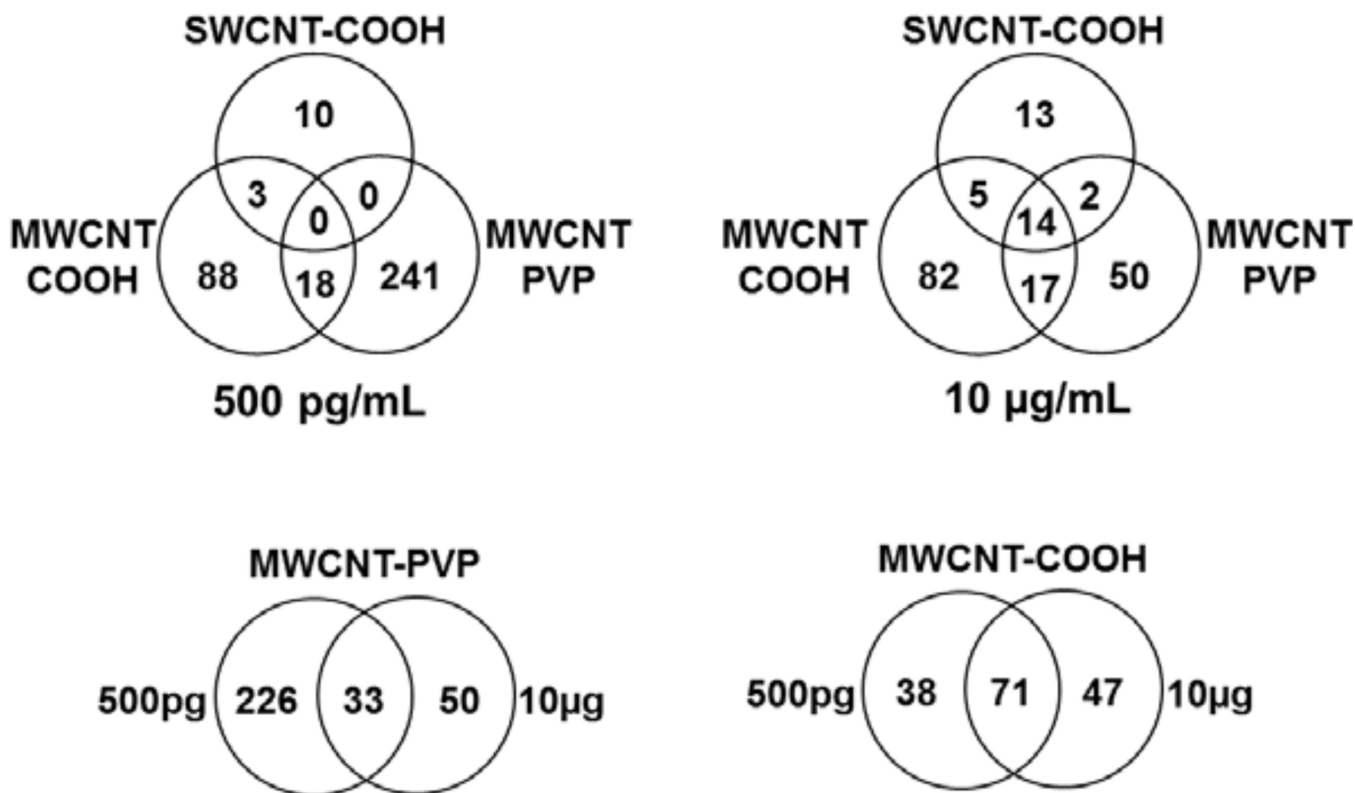
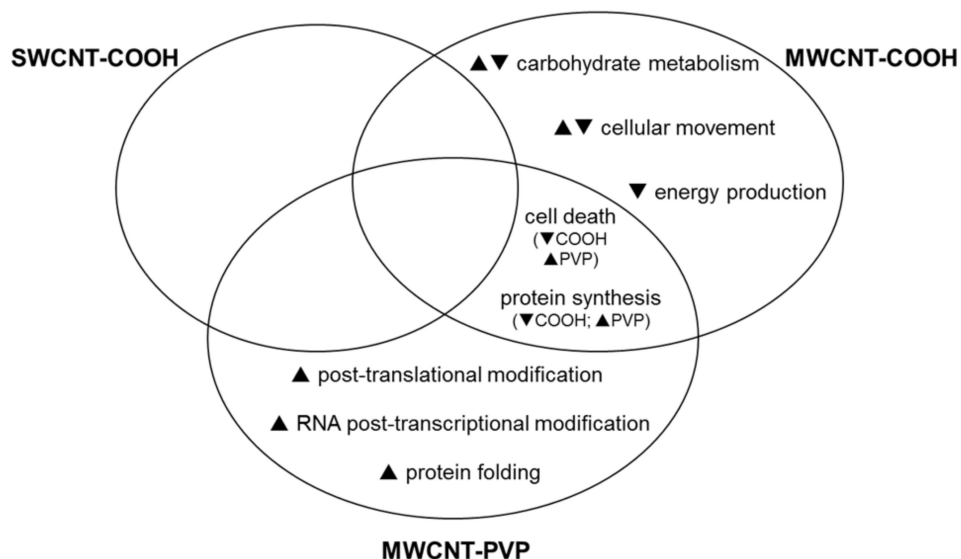


Figure 8.

Venn diagram showing the 428 proteins common or unique to f-CNT treatments

Note: These comparisons illustrate little overlap between the three different CNTs, and only a slightly greater similarity between f-MWCNTs, implying unique cellular effects as measured by differential expression proteomics.

Molecular & Cellular Functions Altered by f-CNT (500 µg/mL)



Molecular & Cellular Functions Altered by f-CNT (10 µg/mL)

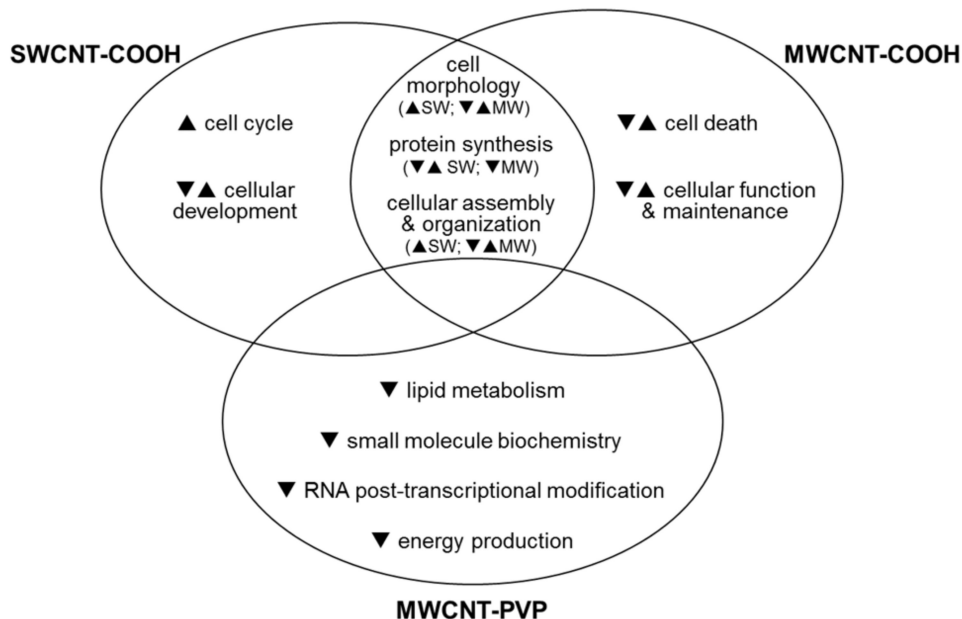
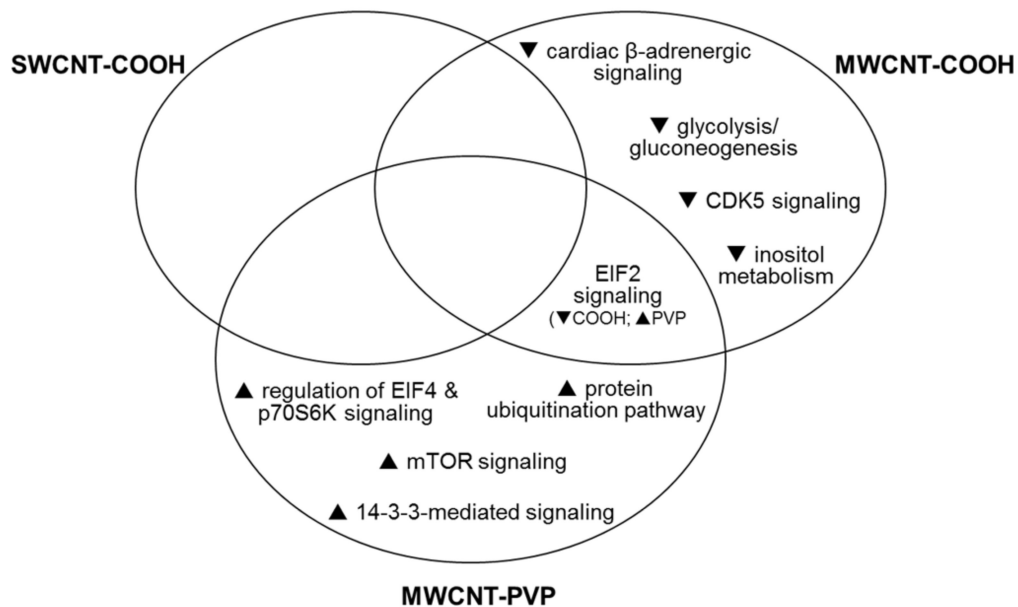


Figure 9.

Venn diagrams showing the molecular and cellular functions common or unique to f-CNT treatments that were most significantly related to the individual protein datasets, as statistically determined by ingenuity pathways analysis

Notes: The general response of proteins comprising those functions is indicated by arrows. As in Figure 8, these comparisons illustrate both the unique functional effects of exposure and functional overlap between the three different CNTs.

Canonical Pathways Altered by f-CNT (500 pg/mL)



Canonical Pathways Altered by f-CNT (10 μ g/mL)

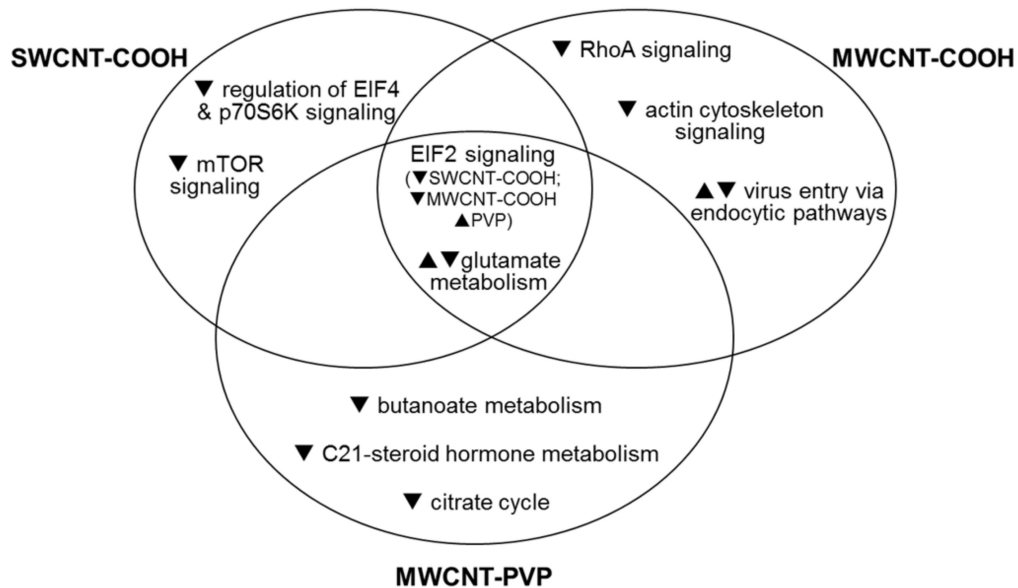


Figure 10.

Venn diagrams showing the canonical pathways common or unique to f-CNT treatments that were most significantly related to the individual protein datasets, as statistically determined by ingenuity pathways analysis

Notes: The general response of proteins comprising those functions is indicated by arrows. As in Figures 8 and 9, these comparisons illustrate both the unique effects of exposure and overlap between the three different CNTs with respect to protein pathways.

Table 1

Physicochemical properties of the f-CNTs

	SWCNT-COOH	MWCNT-COOH	MWCNT-PVP
Outer diameter (nm)	~0.8–1.2	20–30	20–30
Inner diameter (nm)	-	5–10	5–10
Length (μm)	~0.1–1.0	10–30	10–30
Original purity (%)	> 95%	> 95%	> 95%
Zeta potential (mV)	-64.60	-43.70	-42.20
Hydrodynamic size (nm)	211.75	126.40	172.77
Ni content (% weight)	-	-	-
Fe content (% weight)	0.47%	-	-
S content (% weight)	0.93%	0.18%	0.18%

Table 2

Proteins whose expression was altered significantly and similarly by SWCNT-COOH (10 µg/mL) and both exposures to MWCNT-COOH and MWCNT-PVP (see online version for colours)

Gene symbol	Protein name	SWCNT-COOH	MWCNT-COOH	MWCNT-PVP	Function
APIG2	Adaptor-related protein complex 1, 2 subunit	▲	▲	▲	Trafficking pathways between the trans-Golgi network and the cell surface
CEL	Carboxyl ester lipase	▼	▼	▼	Promotes large chylomicron production in the intestine
EIF3C	Eukaryotic translation initiation factor 3 subunit C	▼	▼	▼	eIF3 associates with the 40S ribosome and facilitates recruitment of other eIFs
EIF3F	Eukaryotic translation initiation factor 3, subunit F	▼	▼	▼	eIF3 associates with the 40S ribosome and facilitates recruitment of other eIFs
GCYS-20	Gastric cancer-related protein GCYS-20	▼	▼	▼	Unknown, endonuclease, may specifically degrade the RNA of RNA-DNA hybrids
GFPT2	Glutamine-fructose-6-phosphatetransaminase 2	▲	▲	▲	Regulating the availability of precursors for N- and O-linked glycosylation of proteins
HIST2H2AA4	Histone H2A type 2-A	▲	▲	▲	Nuclear proteins responsible for nucleosome structure of the chromosomal fibre
H2AFJ	Histone H2A.J, isoform 1	▲	▲	▲	Nuclear proteins responsible for nucleosome structure of the chromosomal fibre
H2AFV	Histone H2A.V	▲	▲	▲	Nuclear proteins responsible for nucleosome structure of the chromosomal fibre
H2AFX	Histone H2A.x	▲	▲	▲	Nuclear proteins responsible for nucleosome structure of the chromosomal fibre
HIST1H2BB	Histone H2B type 1-B	▲	▲	▲	Nuclear proteins responsible for nucleosome structure of the chromosomal fibre
H2BFS	Histone H2B type F-S	▲	▲	▲	Nuclear proteins responsible for nucleosome structure of the chromosomal fibre
MIF	Macrophage migration inhibitory factor	▲	▲	▲	Pro-inflammatory cytokine involved in innate immune response to bacterial pathogens
SUCLG2	Succinyl-CoA ligase (GDP-forming) subunit beta	▼	▼	▼	Catalyses conversion of succinyl-CoA and ADP or GDP to succinate and ATP or GTP

Note: Arrows indicate increased ▲ and decreased ▼ expression.